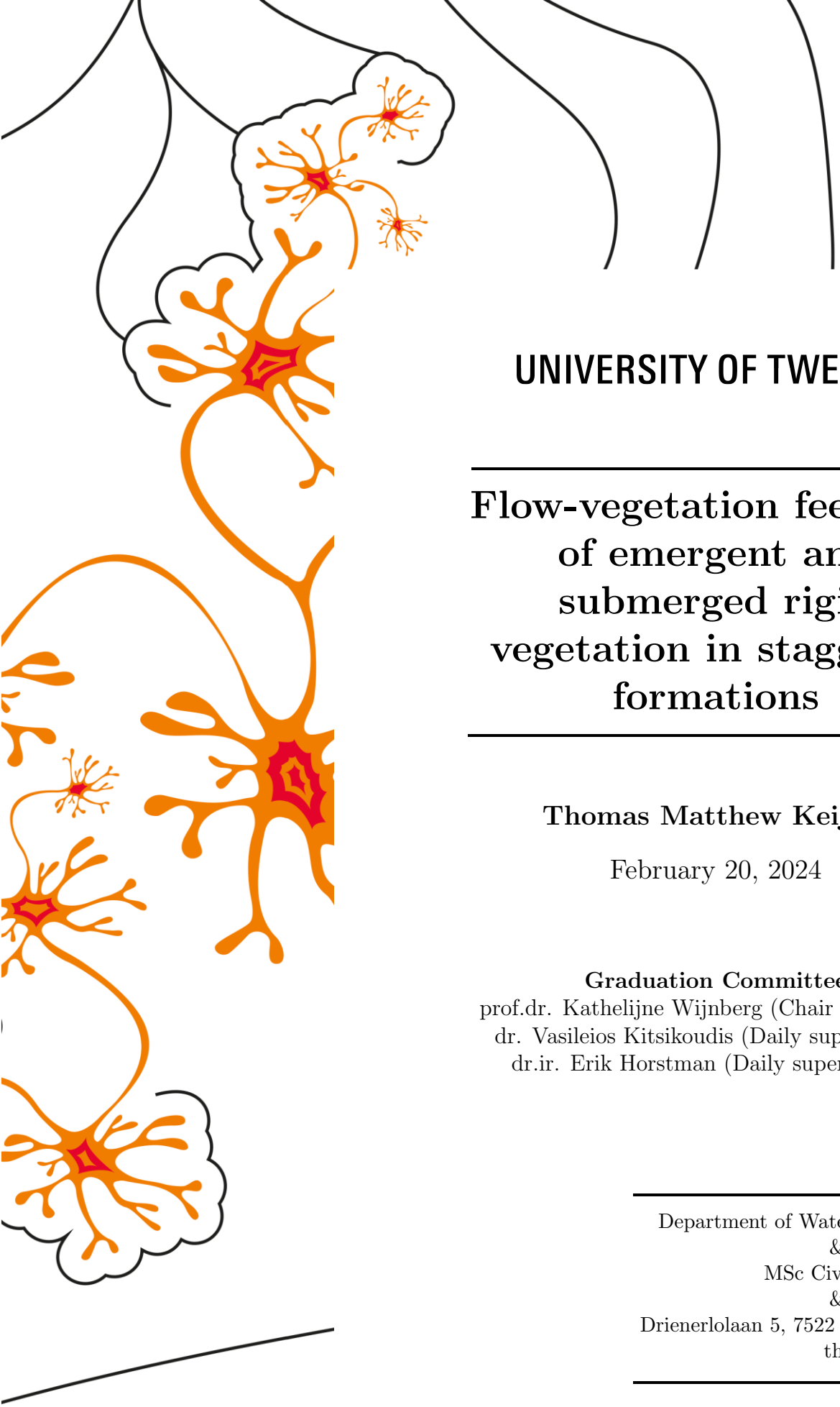

UNIVERSITY OF TWENTE.

Flow-vegetation feedback of emergent and submerged rigid vegetation in staggered formations

Thomas Matthew Keijzer

February 20, 2024

Graduation Committee
prof.dr. Kathelijne Wijnberg (Chair committee)
dr. Vasileios Kitsikoudis (Daily supervisor 1)
dr.ir. Erik Horstman (Daily supervisor 2)

Department of Water Engineering
& Management
MSc Civil Engineering
& Management
Drienerlolaan 5, 7522 NB, Enschede
the Netherlands

Preface

In front of you lies my master thesis "Flow-vegetation feedback of emergent and submerged rigid vegetation in staggered formations". This thesis finalizes my master's degree in Civil Engineering and Management at the University of Twente. An academic journey started at Thompson Rivers University in Kamloops, British Columbia, Canada. Whereafter, I pursued my bachelor's degree in Civil Engineering at the Avans University of Applied Sciences. This academic journey was not the easiest but very fulfilling in the end.

I would like to express my gratitude to my daily supervisor dr. Vasileios Kitsikoudis whose guidance was essential in succeeding in my research. His expertise, love for science in general, and time sacrificed in weekends to provide me with feedback have been essential for my success. You really live to work, thanks Vasileios. Additionally, I would like to thank dr.ir. Erik Horstman for shaping the trajectory of the thesis and being there when needed. Moreover, I would like to express my gratitude to prof.dr Kathelijne Wijnberg for her invaluable contribution throughout this journey in which the end results was not always clear.

Thanks to all the people within the scientific community supporting me in succeeding. I would thank Lennart van Ijzerloo for assisting me in the lab facility of the NIOZ. Also, I would like to thank Mike Jesson for guiding me in the developed software used to despike the data.

My fellow students have been a support in discussions and guidance in the lonely journey. Specifically, I would like to thank Max for being an academic partner since my Bachelor's degree. Having a friend being there throughout my studies will be a foundation for a long friendship to come. Additionally, I would like to thank Hille for the camaraderie throughout this journey.

I am grateful for my family supporting me throughout my academic career and even supporting me when progress was not always constant. I thank my mom for countless times reviewing my writing during this academic career. Translating my thoughts into knowledge was challenging at times, but essential to succeed.

Lastly, to Silke, I am profoundly grateful for you becoming part of my life during my thesis. Your unwavering support has helped me navigate the academic labyrinth, which sometimes felt endless. This gave me perspective when needed. Your support comforted me during the academic stress, thus making success possible.

This thesis symbolizes the collaborative dedication and support which has driven me toward success. The guidance and encouragement from mentors, peers, and loved ones have propelled me. Ultimately showing individual success requires a joint effort.

Thom Keijzer
Enschede, February 20, 2024

Summary

Macrophytes are part of ecosystems within rivers and estuaries. The presence of macrophytes provides a habitat for aquatic life. To be able to provide sufficient management and conservation of these macrophytes, it is crucial to understand the flow-vegetation-sediment feedback. This feedback can influence the evolution of macrophytes within ecosystems and is therefore important in conservation and management. Previous research has explored the flow behaviour of isolated emergent and submerged patches. These experiments have been conducted on rigid and flexible patches. After that, studies have explored neighbouring patch configurations for emergent patches. No research has been done on submerged neighbouring patches. Further research is therefore needed on the interaction between submerged patches to assess how this affects flow behaviour. Ultimately, this will add to the knowledge of flow behaviour around neighbouring patches. Changes in flow behaviour can influence evolution; patches can expand or develop in a new location in space, therefore enhancing ecosystem services within, for example, rivers. This study explores the flow-vegetation feedback of submerged staggered rigid patch configurations in uni-directional flow and aims to show the difference in flow behaviour compared to rigid emergent patches. Additionally, it aims to show the difference between submerged rigid isolated patches and submerged rigid patches in a staggered configuration.

To be able to get an understanding of how submerged rigid patches can influence each other, experiments were conducted at the facilities of the Royal Netherlands Institute for Sea Research (NIOZ) in Yerseke. At the facility, a racetrack flume was used to be able to do measurements on different configurations. Within the flume, two experiments, emergent and fully submerged in staggered configurations, with rigid stemmed patches, were conducted. The interpatch spacing, relative to patch diameter(D), was $2D$ and $0.25D$, respectively, longitudinal and transversal. Reference data for isolated patch experiments from Liu et al. (2018) and staggered emergent patch configuration from Kitsikoudis et al. (2020) were used to compare to experiments conducted at the NIOZ facility. The staggered patches experiments of the reference data had a spacing of $2.5D$ and $0.5D$, respectively, longitudinal and transversal.

For the experiments, an acoustic doppler velocimeter (ADV) was used. To be able to use the collected data, it was crucial to filter the data. Otherwise, contamination of data would influence the results. Within this study, the impact of filters using correlation and signal-to-noise ratio (SNR) on low-quality registered data was explored. Like in other literature, after applying quality thresholds, a 12-point interpolation filled in the missing data points. Good-quality data for the used ADV is considered to have a 70% correlation in combination with 15 dB SNR. These thresholds were applied to the raw data before applying a 12-point interpolation. When the suggested filter for good data was applied, too many data points had to be removed to be able to assess the underlying patterns and behaviours. Too low of a filter would result in too much white noise, and too much of a filter would not leave enough data points to assess flow behaviour. As a result, the -5/3 law of dissipation was used in combination with a power spectral analysis to select the correct filter for the raw data. When using the -5/3 law, the natural dissipation of energy in fluids can be approached. The dissipation of energy in the power-spectral analysis showed an optimal decay when applying a filter of 15% correlation combined with 4dB SNR that was closest to the -5/3 law line of decay.

The water flow behaviour analysis was done using longitudinal and transversal profiles

for both emergent and submerged patch configurations. The main difference between emergent and submerged staggered configurations shown in the longitudinal profiles was the greater turbulence and recirculation behind the submerged patches compared to the emergent patches. Additionally, the transverse profiles showed the same trends.

Overall, the study suggests that submerged patches cause greater mixing due to the vertical vortex behind submerged patches. The vertical vortex of the upstream submerged patch induces turbulence, and when this turbulence is combined with the downstream vertical vortex, turbulence increases even more. This, in part, makes the evolution of submerged patches more difficult than emergent patches, as sediment suspension will likely be greater due to the extra mixing component of the vertical vortex. Also, the velocity is greater behind the submerged patches as flow is not obstructed as greatly compared to the emergent patches. To be able to have the evolution of patches, deposition behind the patches is needed to be able to have the chance for drifting vegetation fragments and seedlings to settle. A greater understanding of the water flow behaviour behind rigid stemmed submerged staggered patch configurations contributes toward the implementation of nature-based solutions in ecosystem development and management.

Contents

List of Symbols

Symbol	Description	Symbol	Description
a	Frontal area per unit	D	Patch diameter
d	Stem diameter	H	Water depth
h	Stem height	I	Turbulence intensity
k	Turbulent kinetic energy	L_1	Length steady wake region
L_{vv}	Steady wake region with vertical vortex	L_w	Length peak turbulence
n	Stem density	u	Flow velocity
u_1	Flow velocity steady wake region	u_e	Exit flow velocity patch
$\overline{u}$	Longitudinal mean flow velocity	$\overline{v}$	Transverse mean flow velocity
$\overline{w}$	Vertical mean flow velocity	ϕ	Solid volume fraction
τ_{xy}	Horizontal shear stress	τ_{xz}	Longitudinal-vertical shear stress
τ_{yz}	Transverse-vertical shear stress	$u\prime$	Longitudinal time average fluctuation
v	Velocity y-axis	$v\prime$	Transverse time average fluctuation
w	Velocity z-axis	$w\prime$	Vertical time average fluctuation
x	Longitudinal coordinate	y	Transverse coordinate
z	Vertical coordinate		

Table 1: List of symbols

1 Introduction

Within rivers, estuaries, and marine systems, aquatic vegetation and plants are present. Macrophytes have an essential role in the functioning of river habitats, the flow of water, sedimentation, and nutrient cycling (Baattrup-Pedersen & Riis, 1999; Kuhar et al., 2011). One characteristic that aquatic vegetation has in common with each other is that it has roots below the water surface. Aquatic vegetation ranges from submerged to emergent, rooted to the bottom surface, to floating vegetation taking its nutrients from the water. Aquatic vegetation, however, has a vital effect on processes like the behaviour of water flow and for example nutrient levels in ecosystems (Cornacchia et al., 2019a). Due to the complex interplay between vegetation and flow an understanding of these processes can help in the effective management and conservation of aquatic ecosystems.

In recent decades, there has been a structural move from flood protection towards the protection and restoration of floodplains; this trend is supported by EU policies (Christiansen et al., 2019). This transition is crucial, as outlined in the Water Framework Directive (WFD), the main law protecting water systems, specifically good quantity and quality of water (European Commission, 2023). Within this directive, it is emphasized that there is a need for effective strategies that balance water safety, ecological health, and human well-being. Within these strategies, both floodplains and the main river channel can be considered in policy choices. On floodplains, trees or bushes can be present, altering flow patterns, for example. In the main river channel, aquatic vegetation, as it is present within a water body, will alter the flow. A contribution towards, for example, water safety can be gained as soil retention is improved due to rooting of this vegetation (Christiansen et al., 2019).

The ecosystem services provided by aquatic macrophytes and nature-based solutions are multifaceted, encompassing benefits such as the provision of habitats for aquatic life, improvement of water quality, and riverbank stabilization (Micheli & Kirchner, 2002; Thomaz & Cunha, 2010). These ecosystem services directly contribute to the well-being of both human and natural life. However, the evolution of freshwater environments has been significantly impacted by human interventions, such as dam construction and river straightening, leading to alterations in sediment discharge and changes in flow patterns (Milliman & Syvitski, 1992; van Vliet et al., 2013). An example of this is intensive land use of floodplains, diminishing natural values and ecosystem services (Jakubínskỳ et al., 2021).

The effect of isolated patches on flow behaviour has been studied extensively, both submerged and emergent (Chen et al., 2012, 2013; Grenier, 2004; Liu et al., 2018; Sadeque et al., 2008, 2009; Zong & Nepf, 2012). Isolated emergent patches have a steady wake region with lower velocities compared to the flow around the patch. At the end of the steady wake region, a Von Karman vortex street will occur when the shear layers start interacting. A Von Karman vortex street is an oscillatory dynamic of large-scale mixing behind an obstacle in a water flow (Hu et al., 2018). This steady wake region makes the deposition of sediment and fragments of vegetation possible (Sand-Jensen et al., 1999). However, with too sparse a patch, the velocity behind the patch will increase as the flow through the patch results in a jet between the individual stems. The deposition of vegetation fragments can cause growth and start the evolution of a patch. Submerged rigid patches have a flow migrating over top of the patch, resulting in a vertical vortex, shortening the steady wake region (Liu et al., 2018). The vertical vortex introduces an additional shear layer next to the shear layers also present at an emergent patch. This

extra-induced turbulence shortens the steady wake region of a submerged patch compared to an emergent patch. Clearly, altering the physical form of a patch can significantly change the behaviour of the flow and therefore, the evolution of patches.

While the presence of aquatic vegetation offers numerous advantages, it also introduces complexities in flow dynamics, which are crucial to understand in order to apply effective management and conservation strategies. Flow-vegetation feedback on patches has been extensively explored in the recent past. This research has explored the impact of both isolated and neighbouring patches, focusing on rigid emergent configurations (Kitsikoudis et al., 2020; Meire et al., 2014; Zong & Nepf, 2012). Understanding the feedback between flow, vegetation, and sedimentation is paramount to understand the evolution of patches in ecosystems, especially in the face of increasing seasonality, differences in maximum and minimum discharge over a year, and altered discharge patterns globally (van Vliet et al., 2013). Building on the understanding of flow-vegetation feedback will contribute to developing informed and sustainable strategies for the management and conservation of aquatic ecosystems in the face of evolving environmental conditions.

Within ecosystems, patches that organize themselves close to each other resulting in minimized hydrodynamic drag (Cornacchia et al., 2019a). When two emergent rigid patches are close enough to each other, they can influence each other's flow behaviour (Kitsikoudis et al., 2020; Meire et al., 2014). This flow behaviour will be influenced by the jet flow present between patches. When patches are too close to each other in side-by-side configuration, the two patches will eventually behave as one bluff body and will therefore share the same Von Karman vortex street for both patches (Meire et al., 2014). In a staggered configuration with emergent patches, spaced both longitudinal and transversal, the upstream steady wake region will be shortened due to the jet flow between the two patches (Kitsikoudis et al., 2020). However, flow behaviour around staggered submerged rigid patch configurations has not been explored yet.

To address the knowledge gaps, this study aims to explore the flow-vegetation feedback of the submerged rigid patch staggered patch configuration in unidirectional flow. The flow behaviour of submerged patches in staggered configuration has not been explored yet in the literature. Macrophytes influence the dynamics of water flow and, therefore, flow patterns. To be able to explore this flow behaviour around submerged patches in staggered configuration experiments will be conducted in this research. These rigid submerged staggered patch configurations also function as an intermediate step in literature towards flexible patch configurations in staggered configurations, as submerged vegetation in rivers and streams is usually flexible.

1.1 Problem Description and Knowledge Gap

Research has delved into the dynamics of water flow across different configurations to gain insights into the flow-vegatation feedback. In literature, the behaviour of flow around isolated patches has been extensively explored (Chen et al., 2012; Zong & Nepf, 2012). Emergent, submerged, rigid-stemmed, and flexible-stemmed isolated patches have all been studied (Liu et al., 2018; Ortiz et al., 2013; Sadeque et al., 2008, 2009; Sand-Jensen & Mebus, 1996; Wang et al., 2022). However, on the other hand, the interaction between patches plays a crucial role in the development of ecosystems. The interaction between two patches, emergent staggered and side-by-side patches, has already been explored in the literature (Chen et al., 2003; Cornacchia et al., 2019a; De Lima et al., 2015; Kitsikoudis et al., 2020; Meire et al., 2014; Yamasaki et al., 2021). The understanding

of flow behaviour and interaction between staggered submerged patch configurations, however, is also crucial to understanding the dynamics of macrophytes in their developing stage before surfacing or macrophytes that remain below the water surface.

In the literature, there is a predominant focus on emergent rigid, neighbouring, and staggered patches. This leaves a void in the understanding of the flow dynamics around neighbouring and staggered submerged patches. Emergent studies have focused on side-by-side and staggered emergent configurations, along with varying densities. Lacking knowledge of the preliminary stages of emergent vegetation, our comprehension of the evolution of macrophytes is limited. To effectively manage ecosystems, the knowledge gap related to the flow-vegetation-sediment feedback process of submerged patch interaction must be closed to gain a greater understanding of the evolution of patches. Therefore, experiments for staggered submerged patch configurations are needed to explore the interaction of these patches in flow dynamics.

Additionally, during the execution of experiments in laboratory settings the data collected in the literature show correlation and signal-to-noise ratio (SNR) above the recommended quality standards suggested by (Nortek Group, n.d.). However, within literature studying the flow around vegetation patches, there has not been research with greatly contaminated data. Applying seeding in experiments can be costly and not every institution is able to bring up these financial resources. Therefore, it is needed to distinguish if it is possible to draw conclusions based on insufficient data quality.

1.2 Research Objective and Questions

In this section, the focus within the knowledge gap, the research objective, and the research questions will be presented. Additionally, for each research question, it will be explained how these will be answered within this study. The pre-existing, reference, data is of high quality and has experiments done with staggered emergent patches. The newly conducted experiments are of lower quality and will have emergent and submerged staggered patch configuration datasets. Both of these datasets will be compared to add to the knowledge gap.

The objective of the research is as follows: *Using new and pre-existing experimental data of experiments to identify the effect on the flow behaviour of neighbouring submerged patches.*

Main research question: How does submergence of rigid vegetation patch mimics in staggered configuration influence flow dynamics of wakes in uni-directional flow?

The main research question concerns solely the submergence of patches within a flow. Various questions need to be asked to understand the flow behaviour occurring to answer the main research question. The elements adding to this question are captured in the sub-research questions below. For each sub-research question, a brief outline will be given of how the research question will be answered.

1. How does data filtering, to take out noise, affect the decay of turbulence and underlying patterns of staggered patch configuration?

   The new data collected in the experiments will need to be filtered, to be able to determine the behaviour of the water flow. Using power spectral density

analysis, the decay of turbulence will be approached as close as possible to the -5/3 law. The effect of filter thresholds before despiking to take out noise will be explored to select the most ideal fit.

2. How do emergent rigid patches in a staggered configuration influence mean flow velocity and turbulence?

   Both pre-existing and new data will be used to answer this sub-research question. Normalized flow velocity, turbulent kinetic energy and transverse turbulence intensity will be determined in both longitudinal and transverse profiles to get an insight into the effect of emergent rigid patches in staggered configurations on the flow. The pre-existing data will be compared with the newly collected data to identify (dis)similarities. Additionally, the behaviour behind the centreline of upstream and downstream patches, using the power spectral density analysis, will be explored to identify differences in profiles of the decay of turbulence.

3. How do submerged rigid patches in a staggered configuration influence mean flow velocity and turbulence?

   Again, both the pre-existing and newly collected data will be used to answer the sub-research question. The emergent reference data of the pre-existing experiments will be compared with the staggered submerged patch configuration of the newly conducted experiments. This will again be done through the same longitudinal and transverse profiles. Again, the differences in the decay of turbulence behind the upstream and downstream patches will compared to see differences in behaviour.

The combination of the sub-research questions' results will be condensed in the discussion and conclusion to answer the main research question. Within the conclusion, recommendations will be made for future research.

2 Theoretical Background

To be able to comprehend the results, a theoretical foundation which supports the research will be shown in this chapter. First, an introduction to macrophytes will be given. This will elaborate on what kind of macrophytes are present in ecosystems and what advantages they give within them. Also, it is explained how these different macrophytes can be compared within literature. Subsequently, the theory on how flow can be quantified will be delved into. This is important as the behaviour of the flow needs to be measured in the various experiments which will be conducted. Lastly, previous research on isolated, side-by-side, and staggered patches will be presented; specifically how different kinds of patches influence flow behaviour. This theory is need to be able to compare the results with the basic behaviour of flow concepts can be recognized in the conducted experiments.

2.1 Macrophytes

Macrophytes, which are essential in aquatic environments, have a range of forms that make them able to thrive in certain environments. Macrophytes largely consist of three main types: submerged, emergent, and floating (Bornette & Puijalon, 2011). Every type of macrophyte has its characteristics that can influence flow patterns and, therefore, its evolution. Often, these macrophytes occur in patches, a well-defined region in which the plant grows (Forman, 1995). As a result of the presence of these patches, ecosystems are shaped physically and chemically. Christiansen et al. (2019) explains how these characteristics create a habitat and therefore provide ecosystem services. Furthermore, plants can alter flow patterns, for example, resulting in the entrapment of particles or reduction of current flow velocities (Madsen et al., 2001). The following subsection delves into the implications of macrophytes on aquatic ecosystems and evolution.

The definition of what a patch is within space can be challenging, but crucial, within research, as pointed out by Schoelynck et al. (2018). The authors explain how within ecosystems, the edge, or boundary, of a patch can be less clear. In Figure 1 it can be seen boundaries of submerged patches, sub-figure **a**, can be harder to distinguish, especially when multiple patches overlap each other. On the other hand, in sub-figure **b** the emergent patch is well-defined and has a clear boundary. Within numerical and experimental studies a patch is often imitated by a construction of individual cylinders positioned in a circular configuration, with a constant density of these individual cylinders within the patch (Liu et al., 2018; Zong & Nepf, 2012).

Emergent macrophytes characterize themselves with rigid stems, anchored beneath the water surface while rising above the water surface. Aquatic vegetation staying beneath the water surface, submerged macrophytes, are typically flexible and streamlined to cope with unidirectional flow, as explained by Bornette and Puijalon (2011). The other main type of aquatic vegetation is floating macrophytes. This can be a macrophyte with floating leaves rooted to the bottom surface or fully floating, where the roots use the water to take up their nutrients and are bound to the bottom (Bornette & Puijalon, 2011).

Macrophytes play a vital role in providing ecosystem services that benefit the environment and the human population. Bytyçi et al. (2022) and Danley and Widmark (2016) describe ecosystem services as a characteristic that benefits human life and their well-being. Ecosystem services can be structures, processes, or benefits provided by nature. An example of an ecosystem service is the increase in water quality when macrophytes take up nutrients in the water; simultaneously, the macrophytes will grow (Micheli &

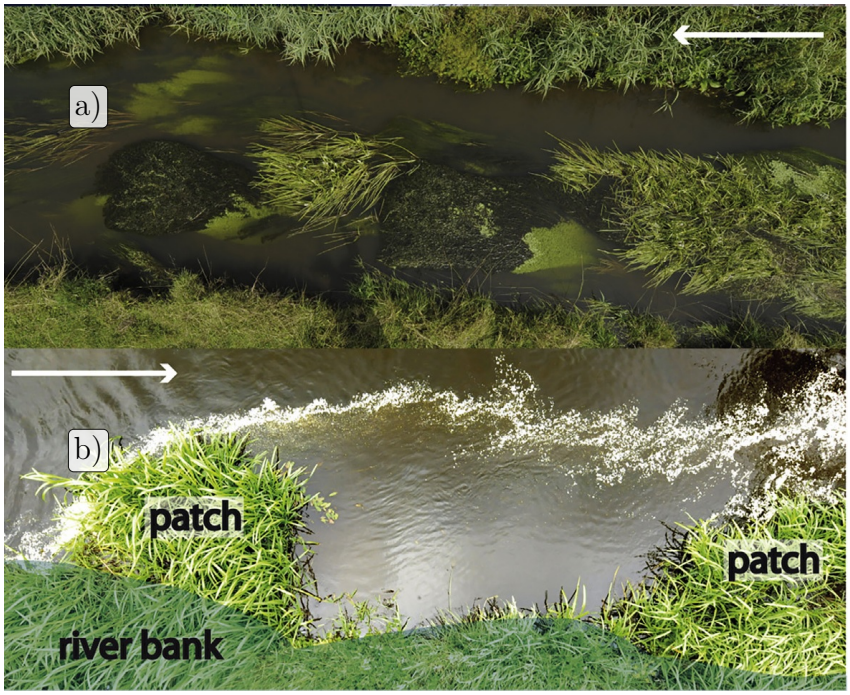

Figure 1: Examples of patches within an ecosystem, the white arrow indicating the direction of flow. Submerged patches are shown in sub-figure **a**. Within these submerged vegetation there are different species present, all having different characteristics. Sub-figure **b** shows an emergent patch with a well-defined patch boundary. Figure adapted from Schoelynck et al. (2018).

Kirchner, 2002). The increase in water quality will make eutrophication less likely. In addition, the plant growth will provide additional habitat for fish (Thomaz & Cunha, 2010). Subsequently, greater biodiversity within the aquatic ecosystem will be present, contributing to human consumptive needs (Chambers et al., 2008). Macrophytes play an important role in preventing the cascading effects of eutrophication within ecosystems. When too many nutrients are available, the ecosystem will change as the turbidity of the water increases (Scheffer et al., 2001). Critical turbidity is reached an ecosystem shift will occur where no vegetation is present due to too high turbidity (Scheffer et al., 2001). Having a sufficient balance of nutrients within ecosystems will guarantee ecosystem services.

Macrophytes alter the flow patterns as flow is deflected around the vegetation (Madsen et al., 2001). With uniform density over the water depth, the near-bed velocity will decrease within and behind the patch, and sedimentation will be promoted (Chen et al., 2012; Kitsikoudis et al., 2016). Along the sides of the patches, the velocity will increase, and erosion may occur. With a treelike patch structure,greater density near the surface and sparser near the bed, erosion patterns will differ as the flow around the patch is altered (Nepf, 2012). Yagci et al. (2016) demonstrates this in their experiments on how different vegetation shapes can influence the scour patterns. What was found is that Reynolds numbers were greater for solid/impermeable objects/vegetation compared to permeable objects/vegetation. As Reynolds numbers change the erosion and evolution will be influenced, for example, a higher Reynolds number implies greater mixing forces on sediment (Kitsikoudis & Huthoff, 2022). Patches evolve due to patch entrapment of sediment and propagules in their wake, causing the growth of macrophytes in the patch's wake (Yagci et al., 2024). This dynamic in time will alter the behaviour of the water flow as the patch characteristics within the flow get altered. A more detailed description of

how patches influence flow will be provided in Section 2.4.

Logically, within ecosystems, there are not solely isolated patches but rather organize themselves patchy (Cornacchia et al., 2019b). The evolution of patches is influenced by patches neighbouring each other and altering each other flow. Cornacchia et al. (2019a) has shown that macrophytes organize themselves in a V-like shape in unidirectional flow. The authors show how macrophytes seem to evolve between 0° and 60° behind an upstream patch. This evolution is primarily a result of drifting vegetation settling in the steady wake region of a patch (Sand-Jensen & Mebus, 1996).

Lastly, aquatic vegetation is often characterized by its density. Within experimental environments or numerical studies, patches often have a constant density within the patch (De Lima et al., 2015; Kitsikoudis et al., 2020). Greater density gives water flow less opportunity to flow through a patch. Lower density logically provides more flow through a patch. To be able to characterize patches, various parameters are found in the literature. The very versatile way of comparing patch densities is the solid volume fraction, ϕ. The solid volume fraction can be determined by using stem density, n, and stem diameter, d, in the following formula $\phi = n\pi d^2/4$. The solid volume fraction indicates the percentage of volume within the patch consisting of solid stem volume. This is a better indicator compared to n as this sole tells you the amount of stems on a bed area and not the amount of flow obstructed. Greater stem diameter d will influence obstruction of flow when increased. Increasing, n and d together will therefore increase ϕ.

2.2 Turbulence

Within the atmosphere, fast-flowing rivers, or even stirring a cup of tea, turbulence is present due to the irregularities within the flow. These irregularities can also be described as fluctuations from the mean velocity (Kitsikoudis & Huthoff, 2022). Turbulent fluctuations that are induced are eddies within a flow (Kitsikoudis & Huthoff, 2022). These eddies therefore cause mixing. To understand the process of mixing fluid, the decay of turbulence must be understood. Richardson (1920) summarized his paper about turbulence in the poem below, which explains the cascade of energy within the flow.

> Big whorls have little whorls
> That feed on their velocity,
> And little whorls have lesser whorls
> And so on to viscosity.
> (Richardson, 1920)

Initially, when mixing occurs as a result of an emergent patch in a uni-directional flow, large-scale eddies will form. These large-scale eddies will add turbulence to the flow and, therefore, extract energy, as seen in the y-axis in Figure 2. As these eddies have the largest integral length scale, they also contain the most energy. Then, eddies will start dissipating into smaller vortices. These vortices will dissipate into even smaller vortices when, eventually the vortices transfer the kinetic energy into heat through viscosity.

This cascade of energy, explored by Kolmogorov, is summarized in the work of Zakharov et al. (2012). In the figure below, this dissipation of energy is visualized in the Kolmogorov energy spectrum. The -5/3 law, proposed by Kolmogorov (1941a, 1941b), describes the energy spectrum of turbulence. For the inertial sub-range, the turbulent kinetic energy (E_k) is proportional to $k^{-5/3}$, k being the wave number. This cascade can be seen in Figure 2.

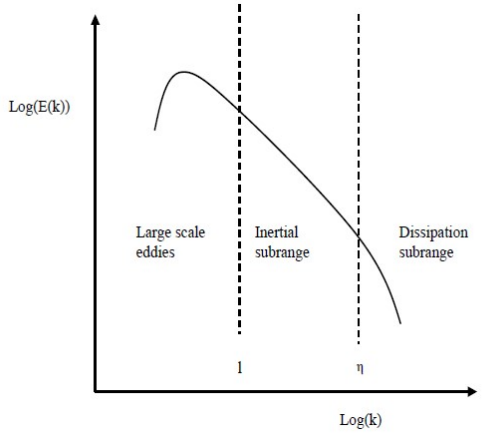

Figure 2: Sketch of the Kolmogorov energy spectrum of homogeneous turbulence, between l and η, respective integral scale and viscous micro-scale. The slope of the dissipation of energy is -5/3. (Shalaby, 2007)

2.3 Quantification of Flow

Understanding the dynamics of water flow requires a physical explanation. The main goal of the physical explanation is to be able to quantify the behaviour of water flow. Typically, quantification of flow is done using a three-dimensional Cartesian system. A Cartesian system, with three axes, consists of a longitudinal (x), transverse (y), and vertical(z) axis. By using these three axes, the flow within water bodies can be characterized. Respectively, the velocities along these axes are represented by u, v, and w. Distortion of these velocity components can cause turbulence, a phenomenon crucial to comprehend when explaining the flow behaviour (Smits, 2000). Within this paragraph, the emphasis is placed on the mean flow velocity and turbulence, as these influence the deposition of sediment and therefore evolution of patches (Meire et al., 2014).

To measure the velocity on the three axes an acoustic Doppler velocimeter (ADV) is often used in research on flow behaviour. An ADV can measure instantaneous velocities of water flow (Meire et al., 2014). Solely instantaneous flow velocity, an observation in time, does not provide an understanding of how the flow behaves. Figure 3 illustrates how time-averaging instantaneous velocities will give an average velocity at a specific point in space. This average velocity is important when determining turbulence in flow, as turbulence within a flow is determined by how the instantaneous velocity differs from the time-averaged velocity.

2.3.1 Reynolds Decomposition

When both time-averaged velocity and instantaneous velocity data are known for a location, Reynolds decomposition becomes crucial. Reynolds decomposition can be applied to determine flow velocity (u) at a specific point and break it down into two components - mean flow velocity ($\overline{u}$) and fluctuation in flow (u'). In Equation (1), the Reynolds decomposition equation, can be seen (Müller, 2006). What is important to note is that the average u', time fluctuations from the mean, is zero. Additionally, this must hold when using fluctuations and average velocity from a single point in space.

$$u = \overline{u} + u' \tag{1}$$

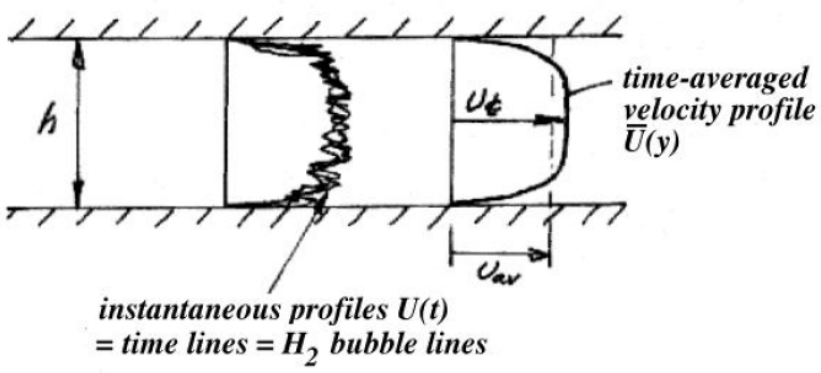

Figure 3: Instantaneous and mean velocity profile in fully-developed channel flow (Smits, 2000)

When getting insight into the flow dynamics of the average scenario, a time-average velocity profile contributes to this. In water bodies, sediment deposition can occur when average flow velocities become small enough. However, it needs to be noted turbulence, and fluctuations in flow velocity, also play a significant role in keeping sediment in suspension (Meire et al., 2014). Therefore, the following can be said, large turbulence in combination with low average velocity can cause the suspension of sediment. Conversely, low turbulence in combination with high average velocity suspension of sediment can also occur. Equation (1), demonstrates the Reynolds decomposition concept in the x-axis. For the other axes, the same concept can be applied. The components for the y and z-axis are the mean velocities, $\overline{v}$ and $\overline{w}$ and fluctuations, v' and w'. Replacing the components in Equation (1) for the different axes gives the ability to quantify the flow for the other axes.

2.3.2 Turbulent Kinetic Energy

The components determined in the Reynolds decomposition can be used to assess the turbulence intensity within a flow. Turbulence is commonly determined by turbulent kinetic energy (TKE), which has units m^2/s^2. TKE indicates the turbulence intensity, with higher values suggesting greater turbulence in a flow. Greater turbulence logically increases the suspension of sediment and lower turbulence increases the chance of deposition of sediment (Chen et al., 2012).

Determination of the TKE involves examining the fluctuations in the flow, denoted as u', v', and w' as explained in the previous section. The TKE, denoted in k in m^2/s^2, can be calculated by using Equation (2) shown below (Lee & Harsha, 1970).

$$k = 1/2(\overline{u'^2} + \overline{v'^2} + \overline{w'^2}) \tag{2}$$

TKE combines the three velocity components' fluctuations, giving a complete measure of turbulence in the flow field. By determining k a valuable insight is given into the behaviour of the flow, directing towards a better understanding of the mechanics of sediments transport and deposition patterns in water flow.

2.3.3 Turbulence Intensity

To determine the magnitude of turbulence in a specific direction of flow, turbulence intensity, I, can be determined. The turbulence intensity is resolved by the fluctuations

relative to the mean flow velocity; these components being taken from the Reynolds decomposition. In equation (3) below turbulence intensity is defined.

$$I_v = \sqrt{\overline{u'^2}}/\overline{u} \tag{3}$$

In Equation (3), $\overline{u'^2}$ represents the time-averaged squared velocity in the longitudinal flow direction. $\overline{u}$ represent the mean velocity at one location, which normalizes $\overline{u'^2}$. When normalizing for various locations, the upstream velocity of the experiment, U_0, can be used instead of $\overline{u}$. As $\overline{u}$ is used to normalize turbulence intensity for one location is space. Applying $\overline{u}$ for all locations in space would not show the relative I to each other.

High turbulence intensity values indicate greater fluctuations with respect to the mean velocity. On the other hand, logically, smaller values show less turbulence is present in the direction of flow. Directions of flow transverse and vertical can be analyzed by using the v and w velocities respectively.

2.3.4 Reynolds Shear Stress

Analyzing shear-induced turbulence caused by shear layers in water flow can be done with the use of Reynolds Shear Stress. Just like the characteristics explained above, Reynolds Shear Stress plays an important role in describing the interaction between different layers of plains within a flow. Reynolds Shear Stress, τ_{ij}, i and j represent directions of flow measurement in the Cartesian coordinate system. The directions used in τ_{ij} logically can be x, y, and z.

Reynolds Shear Stress can be determined in different plains in the three-dimensional space, therefore also in three plains. In Equation (4), the Reynolds Shear Stress for the horizontal plane is shown, with fluctuations in the x and y direction. This horizontal plane shear stress is calculated by using the covariance of u' and v'. The longitudinal-vertical and transverse-vertical plane can be calculated by calculating τ_{xz} and τ_{yz} respectively.

$$\tau_{xy} = -\rho\overline{u'v'} \tag{4}$$

By getting an insight into how the shear stress is present in various directions, the shear layer within the flow can be identified. A negative Reynolds stress indicates a shear layer (Zong & Nepf, 2012). Shear layers indicate a difference in velocity between two planes (Kitsikoudis et al., 2020). In the experiments of Kitsikoudis et al. (2020), it is shown how a positive value shows a velocity difference of the jet flow between patches. A negative shear stress indicates a separated region, such as a steady wake region (Zong & Nepf, 2012).

2.4 Flow Behaviour Patches

Quantification of flow in general can explain the behaviour of a certain physical process within water flow. Within streams, vegetation, emergent or submerged, can be present, affecting the water flow. This vegetation can be present in a patch; a well-defined cluster of vegetation (Schoelynck et al., 2018). These patches can make flow very complex, as flexibility and submergence both influence the behaviour of the water flow. When more parameters are added, the flow patterns become more complex. To imitate patches with rigid stems, a circular array of solid cylinders can be used. This cylindrical array provides flow through the obstacle, like a patch. To gain an understanding of how flow-vegetation

feedback behaves with patches for both isolated and neighbouring/staggered patches, a background will be given below.

2.4.1 Isolated Patches

To be able to explain behaviour around a patch, it is important to understand how a solid cylinder influences the behaviour of water flow, as this does not have flow through the object like patches do. After that, the mechanics of a rigid stemmed patch, also known as a porous cylinder, can be explained. The differences between solid and porous cylinders and their behaviour will become clear for both emergent and submerged patches below.

Solid Cylinder Within fluid mechanics, a solid cylinder is a classic problem which has been researched extensively. Within this research, it is important to understand two situations - emergent and submerged solid cylinders. By delving into the mechanics of water and the interaction of a solid cylinder, insight into the complexities of patches can be gained. Below, the emergent solid cylinder will be elaborated. Thereafter, submerged solid cylinders' influence on water flow will be explained.

Emergent Solid Cylinder As flow approaches a cylinder, different behaviour can occur depending on how turbulent a water flow is. A flow can be laminar or turbulent, both resulting in different interactions with a solid cylinder. A complete laminar flow, with very small Reynolds numbers, will result in no recirculation behind the solid cylinder (Grenier, 2004). The author also describes how when the Reynolds number increases, flow will become turbulent and recirculation behind the solid cylinder can start occurring. Within rivers and streams, it can be assumed water flow is turbulent (Franca & Brocchini, 2015). With both a high enough Reynolds number and flow velocity, Von Karman vortex streets can start occurring. When these occur, these will be present directly behind the solid body (Hu et al., 2018). This phenomenon is large-scale mixing with an alternating pattern behind an object downstream of the wake, as seen in Figure 4.

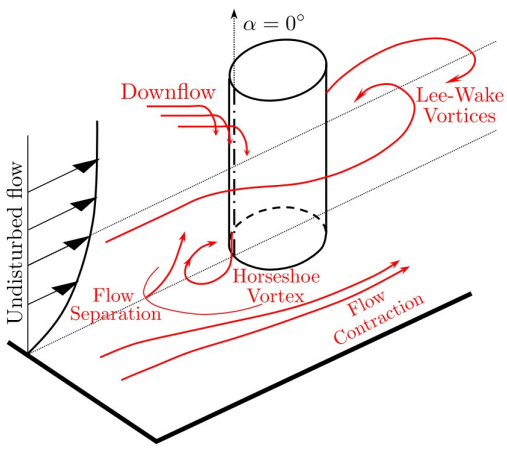

Figure 4: Sketch of flow around a solid cylinder (Kitsikoudis et al., 2017).

When a turbulent flow encounters a solid cylinder, the flow will need to adjust towards the equilibrium condition that the flow had before encountering the solid cylinder. In Figure 5, the mechanics of a turbulent flow encountering an emergent solid cylinder can be seen. As the flow is turbulent, it will oscillate around the mean flow velocity.

When the turbulent flow encounters the solid cylinder, it will move downward and simultaneously move around the cylinder. As the flow moves further down the cylinder, vortex shedding will occur because the flow sheds off the cylinder and lee-wake vortices will form (Kitsikoudis et al., 2016). These lee-wakes vortex shedding occurs when the velocity difference between two layers becomes too great to be able to interact with one another (Sadeque et al., 2008).

When the vortices start interacting, they will form a Von Karman vortex street. Figure 4 shows the beginning of a Von Karman vortex street where the interaction of the vortices results in an oscillating frequency behind the cylinder (Kitsikoudis et al., 2017). The Von Karman vortex street will begin at a certain distance from the solid emergent cylinder, depending on diameter and mean flow velocity.

Submerged Solid Cylinder Flow behaviour becomes more complex when submerging a cylinder as water flow is not only able to move around the cylinder but also over top. The water flow over the top of the cylinder, an additional component, adds a plane resulting in three planes influencing the flow. The behaviour of the flow depends on the relation between water depth H and cylinder height h. When h/H becomes smaller a greater amount of flow can migrate over top of the cylinder.

Sadeque et al. (2008, 2009) studied the behaviour of solid cylinders with different cylinder heights relative to water depth, shown in Figure 5. In Figure 5 **a** to **d** Von Karman vortex street is not formed due to the great flow overtop of the submerged solid cylinder, resulting in a vertical vortex downward, creating a shear layer, in the z plane. Both of these solid cylinders are fully submerged with a h/H ratio of 0.25 and 0.55. When a solid cylinder is slightly submerged, $h/H \approx 0.9$, the vertical vortex is not significant enough to destroy the Von Karman vortex street.

Rigged Stemmed Patches In research, rigid emergent stemmed patches are often used in flume experiments to imitate emergent macrophytes. These macropythes are often resembled by a cylinder-shaped patch with individual stems, making a porous cylinder (Chen et al., 2012; Kitsikoudis et al., 2020). Porous cylinders show similar behaviour to solid cylinders when patches are dense enough (Kitsikoudis et al., 2016). However, the dynamics are more complex due to the bleed flow through the porous cylinder (Chen et al., 2012).

Emergent Rigged Stemmed Patches When the density of emergent rigged stemmed patches is high enough, Von Karman vortex streets can be present in turbulent flow (Kitsikoudis et al., 2020). The vortex street can occur when enough water flow propagates around the porous cylinder. Therefore, for a Von Karman vortex street to occur, a sufficient density of the individual stems within the patch is needed (Takemura et al., 2007). Similar to solid cylinders, the flow around the porous cylinder causes shear layers, also seen in Figure 6. The distance at which these shear layers start to interact, the formation distance, is greater compared to solid cylinders due to the bleed flow through the porous cylinder (Hu et al., 2018). Lower density results in a greater steady wake region L_1 and a greater velocity, U_1, within this region. At the upstream end of the steady wake region, the exit velocity of the bleed flow through the patch, U_e, is always slightly greater compared to U_1 (Chen et al., 2012).

The wake vortices of a porous cylinder become less apparent when more bleed flow is present and less flow around the cylinder is present. This greater bleed flow will

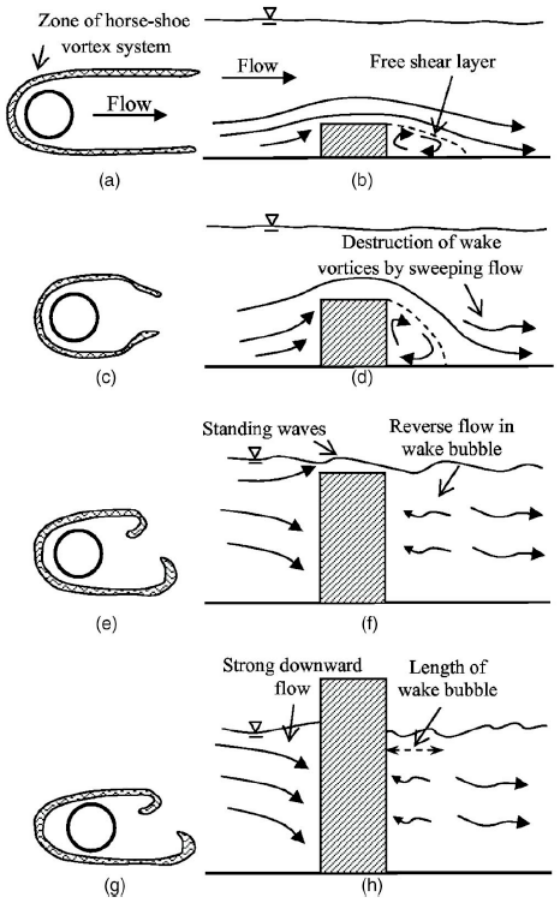

Figure 5: Sketches on vortex system and flow on the plane of symmetry with respect to solid cylinder in water depth (H) of 220 mm. Cylinder height (h) varies, a-b h: 55 mm, c-d h: 120 mm, e-f h: 200 mm, and g-h h: 300 mm (Sadeque et al., 2008)

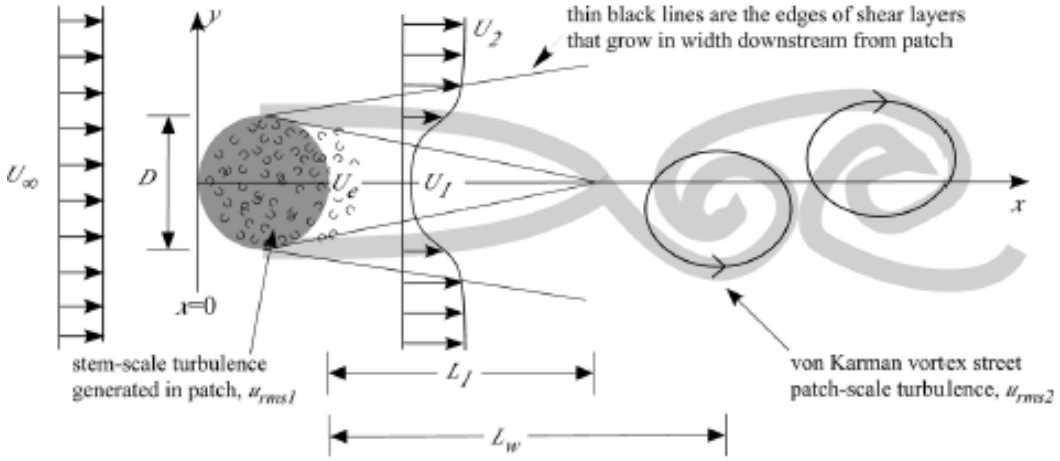

Figure 6: Flow through and around an emergent vegetation patch. U_∞, called U_0 in text, showing incoming flow velocity. Within the steady wake region U_1 showing velocity and L_1 the length of the region. U_2 is increased as flow is diverted around the patch. L_w indicates length towards the peak of the turbulence behind the patch (Chen et al., 2012)

enhance the length of the deposition region, as the shear layers will start interacting further downstream. However, when the porous cylinder becomes too sparse, there will

start being primitive Von Karman streets of the individual stems within the steady wake region, but the main Von Karman street of the emergent rigid stemmed patch will stay present (Takemura et al., 2007). The authors further explains that when the sparseness is too great, no Von Karman vortex street will remain, and only the primitive Von Karman vortex streets of the individual stems will remain.

Submerged Rigged Stemmed Patches Like submerged solid cylinders, rigged stemmed patches that are submerged have similar behaviour when the density is great enough. Just like with a solid cylinder, the flow will have a vertical deflection upward when coming into contact with the obstacle, as seen in Figure 5. Thereafter, when the downstream edge of the submerged patch is reached, a vertical vortex downward will be present. This similar behaviour can be observed in Figure 7.

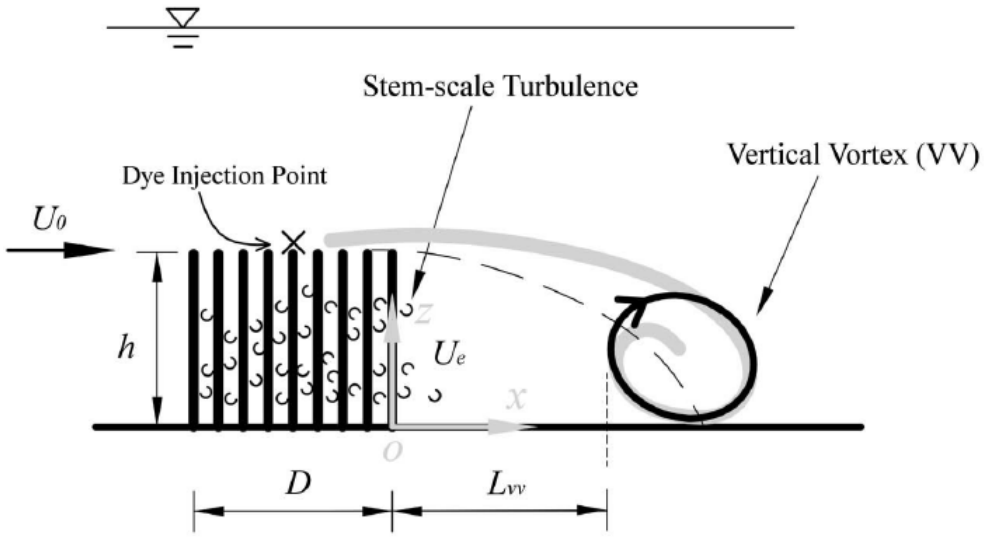

Figure 7: Flow around a submerged rigid stemmed patch. U_0 showing incoming flow velocity. U_e shows exit velocity from patch. Vertical vortex is shown by recirculation in black. The steady wake region,L_{vv}, is the distance from the trailing edge of the patch up to vortex in the vertical plane (x-z plane) (Liu et al., 2018)

When a vertical vortex is present, the water flow moving over top of a submerged, rigid stemmed patch will shorten the deposition region. This is due to the induced downward shear layer, which causes turbulence. A smaller h/H ratio will result in a shorter deposition region (Liu et al., 2018). Liu et al. (2018) also points out that a greater patch diameter will result in a larger deposition length. The shear layers caused by a cylinder will need a greater distance from the path to start interacting with each other. In the experiments of Liu et al. (2018), however, it is shown that when the h/H ratio becomes small enough, 0.21, the diameter will not influence the deposition length; for different patch diameters, the deposition length is equal. When a Von Karman vortex street is present the deposition length will increase with greater patch diameter D.

The differences compared to solid cylinders are due to the presence of bleed flow through the patch. The distance at which shear layers start interacting, L_{vv}, as seen in Figure 7, is greater as a result of the bleed flow. Just like with the emergent porous cylinders, the steady wake region will increase when the sparseness gets greater (Liu et al., 2018).

Von Karman vortex streets can occur when the density of the patch is sufficient. In the experiments of Liu et al. (2018) the effect of submergence of porous cylinders on Von Karman vortex streets has been studied. In the authors' experiments, a constant frontal area per unit volume, a, and stem density, n, were used, respectively 0.51 cm^{-1} and 1.43 cm^{-2}. n shows the amount of stems per bed area. These values indicate how dense a patch is, when the value increases so does the density. Liu et al. (2018) found that a Von Karman vortex street appeared when $h/D < 0.7$ and was absent when $h/D > 0.7$. What can be expected is that this ratio will increase when the density of the patch decreases, as the shear vortices of the flow going around the patch will become less intense.

2.4.2 Neighbouring Patches

Isolate patches have been studied extensively. To add to the behaviour of isolate patches, explained above, the interaction between side-by-side and staggered patch configurations will be explained below.

Side-by-Side Patches Initially, solid cylinders have been used to study the effect on flow behaviour in side-by-side configuration. Chen et al. (2003) showed that at a substantial spacing, of three times the patch diameter D, solid cylinders do not show any influence on each other's Von Karman vortex streets. Sumner (2010) exhibited that at closer proximity, $2.2D$ still no influence was observed. However, when the spacing is decreased to $1.7D$ deflection is observed in the gap flow between the solid cylinders (Chen et al., 2003). This deflection causes a "flip" of the Von Karman vortex streets as they start influencing each other. When the spacing of neighbouring solid cylinders falls below $1.2D$ the two bodies will act as one single bluff body and therefore have one Von Karman vortex street (Sumner, 2010).

Vandenbruwaene et al. (2011) studied side-by-side patches with live vegetation. The experiments were done in square patch configurations, but this did not have significant effects on the results compared to circular patches. The author found that patches started interaction at $D/d >= 0.43-0.67$, where D is patch diameter and d is interpatch distance. At $D/d >= 6.67 - 10$, the patches started behaving as one bluff body. This distance is closer to each other compared to the solid cylinders as flow suppression is less for permeable vegetation.

Meire et al. (2014) has revealed how neighbouring rigid emergent patches can influence flow behaviour and deposition. Similar to isolated emergent patches, L_1 is influenced by the density of a patch. A sparser patch results in a longer steady wake region, L_1 (Meire et al., 2014). On the other hand, Meire et al. (2014) points out that when increasing patch density, the flow velocity increases between patches, and the minimum flow velocity further downstream is lower compared to sparser patches. Both Kitsikoudis et al. (2020) and Meire et al. (2014) found the merge of the wakes of the two patches further downstream was located where the velocity came to a local minimum on the centerline. As a result, deposition is promoted in these locations in space. Kitsikoudis et al. (2020) points out that neighbouring patches most likely do not have the same density, leading to an asymmetry in the jet between the patches. In the research of Kitsikoudis et al. (2020) this asymmetry in the jet is a result of the greater diversion of flow for a dense patch compared to a sparser patch, in part causing an asymmetry in vortices.

Staggered Patches In natural settings, patches are more likely to grow in V-formations as pointed out by Cornacchia et al. (2019a). Kitsikoudis et al. (2020) illustrates how in staggered emergent rigid patches, a downstream patch shortens the upstream patch's steady wake region. The upstream wake is shortened due to the flow diverted between the patches. Additionally, when the downstream patch's density becomes greater, the upstream steady wake region will become shorter (Kitsikoudis et al., 2020). The author also adds that the Von Karman vortex street will be distorted.

The experiments of Kitsikoudis et al. (2020) have all been conducted at a transverse interpatch spacing of $0.5D$ and longitudinal interpatch spacing of $2.5D$. De Lima et al. (2015), however, investigated in a numerical study at what spacing interaction of staggered patches is present. What was found by the authors is that, with a constant frontal patch density of $\phi = 0.3$, no interaction was observed with transverse and longitudinal spacing, respectively $1.5D$ and $5D$ centre-to-centre distance.

3 Methodology

Within this study results of (new) experiments and of previous experiments, reference data, will be analyzed. First, the experimental of the (new) experiments conducted at the facilities of the Royal Netherlands Institute for Sea Research (NIOZ) will be elaborated. These experiments conducted at the NIOZ are both emergent and submerged patches in staggered configurations. Thereafter, the parameters in which the previously conducted experiments of the reference data have been done at the Hydraulics Laboratory of Istanbul Technical University will be presented. Lastly, the ADV setup used at the NIOZ will be presented.

3.1 Experimental Setup NIOZ

The flume at the Royal Netherlands Institute for Sea Research has been used to conduct the experiment and collect data for the emergent and submerged cases. In the flume, various setups have been used to gain a greater understanding of flow-vegetation feedback. In the experiments, the instantaneous speed of the flow has been measured to determine the behaviour of the water movement.

3.1.1 Racetrack Flume NIOZ

The racetrack flume at the NIOZ facility provides the possibility to do experiments in various patch configurations with the same flow conditions. First, the flume itself will be introduced. After the fixed parameters are shown, the experiments will be explained.

The flume is a uni-directional flume driven by a drive belt, as seen in Figure 8. The dimensions are 17.55 m in length by 3.25 m in width. In the bottom straight there is a carriage situated which caries the measuring instrument, as seen in the figure. Using this equipment measurements can be done within the test section. The test section has a clear glass wall and a lowered bed. Logically, the glass wall provided a side view of the experiment. The lowered section gives the possibility of having the setup of the experiment at the same height as the flume bed. The width of the flume, and more importantly, the test section, is 60 cm. The width of the flume will determine the size of the setup, as interference from the wall will need to be accounted for. An extensive explanation of the racetrack flume is given by Bouma et al. (2005).

Within the flume, a wooden construction has been assembled to be able to make the different configurations. The wooden construction holds the stems of the various setups. The stems were made from carbon sticks, which were cut to the desired length. The experimental setup in the flume is constructed from 18 mm plate material, which is concrete-plex. The plate has holes drilled in it in the desired locations to hold the stems of the patches. The holes were made approximately 10 mm deep, so this extra length could be accounted for when cutting the carbon sticks. Three platforms have been made two short ones 59·122 cm, platform 1 and 3, and one large one 244·59 cm, platform 2, which bridges the lowered section in the flume at the NIOZ facility. A schematic top view is shown in Figure 9. The remaining centimetre difference between the flume and the plate was filled in situ with high-pressure laminate (HPL) plates on one side of the flume so no flow would go between the minimal gap during the experiments. Beams, 44·70 mm spruce, are mounted on the bottom of these plates to provide stiffness. Additionally, the beams provide a mounting point for the legs. The legs are also constructed from concrete-plex and have a 'shelf' to hold ballast, so the platform is kept submerged during

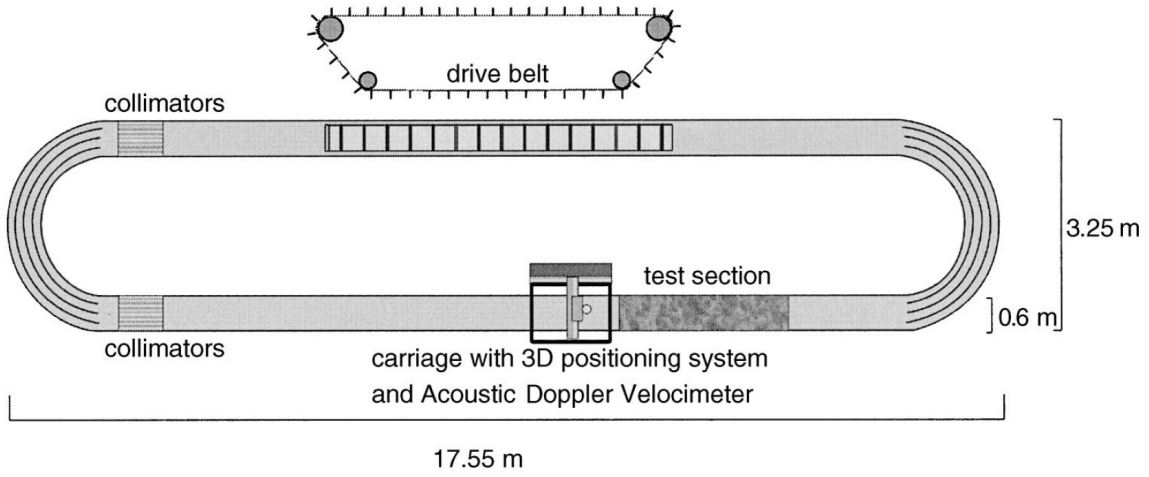

Figure 8: The racetrack flume used for flow-vegetation feedback in uni-directional flow. The direction of flow is from left to right in the test section, situated in the opposite straight of the belt drives straight (Bouma et al., 2005)

1 (122 · 59 cm)	**2** (244 · 59 cm)	**3** (122 · 59 cm)

Figure 9: Schematic top view of the three constructed platforms. The middle one bridges the lowered section in the flume of the facility of the NIOZ.

the experiments. The height of the total structure is 16.5 cm. By doing this the total water depth within the flume was 30.5 cm, this also helped the belt drive of the flume to function better as the belt could not move downward far enough to propel a minimal water depth.

Having the same flow conditions approaching the obstacles — the patches in this case — is essential to be able to compare the difference in behaviour across the different setups. In Table 2 a summary of the fixed conditions in the experiments is shown. Below the table, an explanation of the choice of fixed parameters is provided.

Table 2: Fixed parameters flume experiment

Parameter	Value	Unit
Water depth (H)	0.14	m
Flow velocity (U_0)	14	cm/s
Patch diameter (D)	0.07	m
Stem density (n)	1.49	cm^{-2}
Solid volume fraction (ϕ)	0.149	-
Circular cylinder diameter (d)	0.003	m

3.1.2 Patch Configuration

For the patch configurations, various setups of patch mimics have been used. These vegetation mimics represent patches within a flow. Two setups have been analyzed at the facilities of the NIOZ. First, the characteristics of the patch used will be discussed. Thereafter, the patch layout will be presented.

Patch Characteristics The patches have been designed to be able to function within the limitations of the flume situated at the NIOZ. The parameters considered in the design of the patch are width and solid volume fraction. In Figure 10 the pattern used to mimic rigid vegetation in the flume is shown. The choices made on the patch design are elaborated below.

The structure of the patch consists of 81 stems. The outside diameter of the patch is 7 cm, with individual stems of 3 mm. As mentioned in the previous section, regarding the racetrack flume, the width of the flume is what limits patch size. The diameter of the patch compared to the width is comparable with experiments done by Kitsikoudis et al. (2020) and Meire et al. (2014), where in both cases approximately 9 % of the flume width was used for the patch size. With this patch diameter and the 60 cm flume width, this ratio is approximately 12 %. The patchs' stems are distributed evenly over four radii with one center point/stem. The first radius, closest to the center stem, has eight stems evenly spaced. Every next radius towards the outside has an additional eight stems. With these characteristics, the patch has a solid volume fraction, ϕ, of 0.149. This value of ϕ, frontal volume fraction, has a value between the medium and dense patches defined in the experiments of Kitsikoudis et al. (2020). The experiments of Liu et al. (2018) used a very comparable solid volume fraction, ϕ, of 0.15. When compared to the experiment of Meire et al. (2014), the solid volume fraction is greater. The chosen characteristics strike a balance between capturing relevant dynamics and ensuring comparability with previous studies, rendering the patch suitable for the research objectives. The selected flow velocity was 14 cm/s, at this velocity Von Karman vortex streets have been observed making it suitable for the objective of this research.

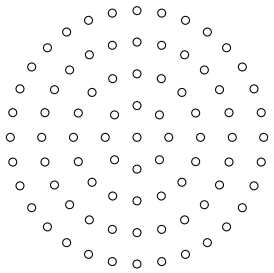

Figure 10: Design of patch used in the experiments at the NIOZ facility. Patch diameter, D, of subfigure is 7 cm with stem diameter, d, of 3 mm.

Patch Layout To effectively assess the behaviour of flow in response to patches, it is important to position these patches precisely in each configuration. This is especially important as the experiments conducted at the NIOZ facility have different stem heights, h, with the same position. The different stem heights are: emergent and fully submerged. As mentioned in the fixed parameters, the water depth, H, will be 14 cm. Therefore, the stem heights, h, respectively are 16, and 7 cm. Below in Table 3 the setups are

summarized for experiments conducted at the facility of the NIOZ. An overview of the various positions is shown in Figure 13. Below the table, detailed explanations and considerations regarding the configurations are provided.

Table 3: Configuration flume experiment

Case	h (cm)	h/H	centre *(x-y)* position downstream patch	centre *(x-y)* positions upstream patch
Staggered emergent	16	1.14	(-0.5,-0.625)	(-3.5,0.625)
Staggered fully submerged	7	0.5	(-0.5,-0.625)	(-3.5,0.625)

The longitudinal and transverse spacing has been made smaller in comparison with the experiments of Kitsikoudis et al. (2020). In their experiments a longitudinal interpatch spacing of $2.5D$, along with a transverse interpatch spacing of $0.5D$ has been used. Within the experiments, the jet flow between the patches was not significant. Therefore, to strengthen the jet flow the interpatch spacing has been decreased to $2D$ and $0.25D$, respectively longitudinal and transverse. This increased jet flow is also important as the vertical vortex of the fully submerged configuration also shortens the steady wake region. For patch height two heights are considered in the experiments, $h/H = 1.16$ emergent, and $h/H = 0.5$ fully submerged. Liu et al. (2018) considered these same h/H ratios in their experiments with isolated patches. Additionally, the solid volume fraction between the patch design shown in Figure 10 and the isolated patches in the experiments of Liu et al. (2018) have almost identical solid volume fractions.

3.2 Experimental Setup Hydraulics Laboratory of Istanbul Technical University

To be able to do a sufficient comparison with the acquired data at the NIOZ facility, it is important to elaborate on the conditions used in the provided data. First, the flume will be discussed. Thereafter, the patch configuration which was used will be elaborated on.

The reference data used in the results is provided from experiments conducted in the recirculating Flume Hydraulics Laboratory of Istanbul Technical University. The flume is 0.98 m wide with a depth of 0.85 m. The bed is constructed of smooth concrete with plexiglass walls. Kitsikoudis et al. (2016) provides a more extensive description of the flume.

At the facilities of the Hydraulics Laboratory of Istanbul Technical University Kitsikoudis et al. (2020), data for all possible combinations of staggered configurations with sparse, medium, and dense patches has been collected. Besides, the staggered configurations, neighbouring, and isolated patches have been investigated in the research of Kitsikoudis et al. (2020). For the reference data's experiments, the staggered configurations of Kitsikoudis et al. (2020), medium and dense. Respectively, these solid volume fractions are 1.14 and 1.88. The solid volume fraction, ϕ, used in the 'new' experiments is 0.149. The medium density used by Kitsikoudis et al. (2020) is below this solid volume fraction. Additionally, the dense patch of the reference data's solid volume fraction is

above that of the 'new' experiments. Below, the characteristics are summarized in Table 4.

Table 4: Fixed parameters flume experiments Hydraulics Laboratory of Istanbul Technical University

Parameter	Value	Unit
Water depth (H)	0.30	m
Flow velocity (U_0)	24.4 ± 0.3	cm/s
Patch diameter (D)	0.09	m
Solid volume fraction medium-density patch (ϕ)	0.114	-
Solid volume fraction dense-density patch (ϕ)	0.188	-
Circular cylinder diameter (d)	0.005	m

The staggered configuration used in the experiments of the reference data has different longitudinal and transverse spacing compared to the experiments done at the NIOZ. The $x-y$ position of the downstream patch is (-0.5,-0.75) and the upstream patch is (-4,0.75), where $x = 0$ is the downstream edge of the downstream patch.

In conclusion, the reference data collected by Kitsikoudis et al. (2020) at the facilities of the Hydraulics Laboratory of Istanbul Technical University can assist in determining trends in the data collected at the NIOZ. These trends can be valuable as the reference data has similar conditions to the experiments done at the NIOZ facility.

3.3 ADV Setup

Determining flow velocities in water flows is commonly done by the use of an Acoustic Doppler Velocimeter. The ADV records the flow velocities in three dimensions, x, y, and z-axis. The instrument measures the velocity of the particles in the water using the acoustics beams. The instrument in mounted to a carriage to be able to measure at different positions, longitudinally, in the flume. In Figure 11 a picture of the carriage is shown.

In the facilities of the NIOZ, seawater from the Oosterschelde is used. This seawater contains a myriad amount of suspended particles, both sediment and algae, which are needed to do measurements with the ADV measuring probe. As this acoustic instrument uses particles' reflections to determine the velocity of water in a specific direction. The measurements are taken 5 cm below the probe transceivers, the CNC arm accounts for this in the software used at the institute. The CNC arm can take measurements of 60 cm in the longitudinal direction on each run, as these are the limitations of the reach of the x-axis of the arm. To be able to measure the adjacent 60 cm, the carriage, which holds the CNC arm, needs to be moved. The three sections used within the limitations of the carriage are shown in the overview in Figure 12. Within the software of the CNC arm, coordinates can be entered to automate these measurements within each test section. At each coordinate, measurements of the instantaneous velocity of the water are taken for 180 seconds with a frequency of 100 Hz. This frequency is equal to the frequency used by Kitsikoudis et al. (2020). Measurements are taken 3 cm above the bed of the construction. No seeding was used as it would be too costly, and suspended particles was plentiful when filling the flume.

Figure 11: Carraige photographed from the upstream position looking downstream. The CNC arm is mounted on the left side of the carriage, the vertical axis of the arm positioned above the water has the ADV sensor attached to it. The legs on each corner have wheels mounted to be able the move the carriage between the various test sections.

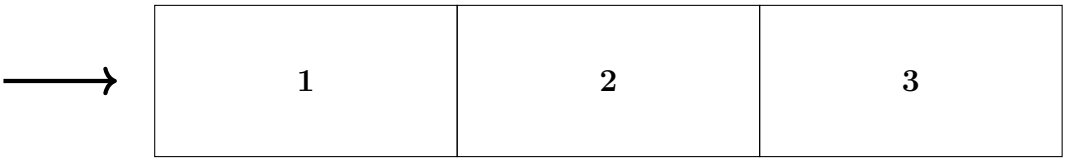

Figure 12: Test sections to correspond with the limitations of the carriage. The direction of flow is indicated by the arrow. Test section 1 contains the patches in staggered configuration. Test sections 2 and 3 are further downstream from the patches.

To do measurements, a carriage with an Acoustic Doppler Velocimeter (ADV) mounted to a computer numerically controlled (CNC) arm can take measurements of the flow. By programming the CNC arm measurements can be taken at the desired locations for the required amount of time. The measurements of the ADV are done in a sampling volume 5 cm below the instrument (Nortek Group, n.d.). This makes measurements impossible in the first 5 cm from the water surface downward, as the acoustic signals need to travel through water. This is taken into consideration with the sampling pattern.

Within the computer program of the CNC arm coordinates are put in so that measurements can be taken at these coordinates. Near the patches, greater detail is needed as more changes in flow behaviour take place here. Further downstream from the patches, the flow goes back to an equilibrium, so less detail is required. In Figure 13, the coordinates relative to patch diameter D are shown. The centerline in between the patches has the y coordinate zero. The downstream edge of the downstream patch is marked as zero on the x-axis. In the figure, **a** and **b** respectively, the x-y position relative to the diameter, D, of the measurements and z position relative to the water depth, H, can be seen.

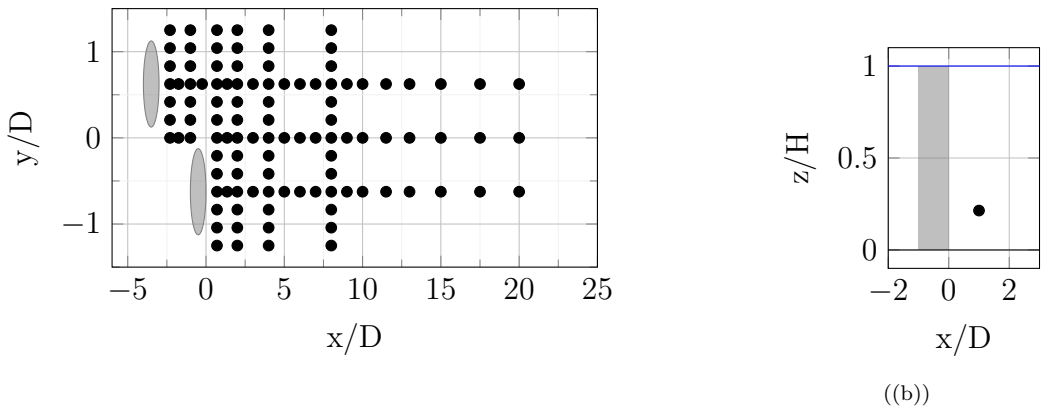

((a)) ((b))

Figure 13: Measuring locations ADV, flow direction from left to the right. Patches are indicated by grey circles or column. (a) top view plane of locations of ADV measurements, indicated by black dots, isolated configuration (b) side view heights of planes for measurements, indicated by black dots

When using a measuring instrument, inaccuracies can occur for various reasons in data recording. When using an ADV within a flume, different factors can adversely affect the data recording. During the recording of the data, 'weak spots' result in lower signal noise ratio (SNR), correlated values, and noisy velocity traces (Nortek Group, 2022). Nortek Group (2021) explains that this will solely happen at certain distances from the probe depending on the velocity range setting. A different example of a problem which can occur is the interference of highly reflective bottoms (Nortek Group, 2022). Highly reflective bottoms, which have a large return of signal, can pollute the water column and result in the possibility of getting unreliable data. Considering the concrete-plex used for the bottom surface of the experiment, this could be a problem. Additionally, within basins or flumes, seeding is often needed due to lack of suspended sediment (Nortek Group, 2022). Lastly, pulse-coherent instruments can have errors in the data recordings in phase wrapping or aliasing (Goring & Nikora, 2002; Nortek Group, 2022). Phase wrapping occurs when signal interference happens between the first and the second pulse, causing phase ambiguity as the returning echo cannot distinguish between the two pulses (Goring & Nikora, 2002; Nortek Group, 2022). To be able to assess the results errors like these need to be filtered to have usable data to interpret.

Using the same parameters for the measurements done by the ADV contributes to a good comparison of configurations. The CNC arm, which is of great accuracy, facilitates this goal within the experiments. The limitations of the ADV have been considered in the setup of the probe, by not being in the range of signal interference for example.

4 Results

In this section, the results will be analyzed using the data collected and provided. For the experiments executed at the NIOZ the spacing, both longitudinal and transversal, is constant. For the conducted experiments at the NIOZ respectively, the patches in the configurations have a height, h, compared to a water depth, H, of $h/H \geq 1$ and $h/H = 0.5$. First, the data filtering done on the unexpectedly low-quality, contaminated data will be analyzed to select the most ideal filter thresholds for despiking the data. By doing so the underlying patterns and behaviour is guaranteed as much as possible. Thereafter, a power spectral density analysis comparison between various positions will be done to determine a difference in behaviour between upstream and downstream patches. Next, longitudinal and transverse analyses of the flow behaviour have been done. By doing so the flow dynamics in the wakes of the patches, both submerged and emergent, can be determined. Below, all analyses are elaborated.

4.1 Despiking Data

The following section is devoted to a comprehensive power spectral analysis, which is required due to the unexpectedly low data quality of the acquired data at the facilities of the NIOZ. Within the determination of the behaviour of the water flow, it is important to have data that has the same rate of dissipation of turbulence as proposed by Kolmogorov (1941a). When dissipation of turbulence is greater underlying behaviour and trends of the water flow will be filtered out. The aim is therefore to achieve a balance between taking out enough noise and keeping the underlying patterns of the flow behaviour, within the limitations of the data quality.

Before doing any detection and replacement of spikes, Nortek Group (2022) suggests screening out insufficient data below $\approx 70\%$ correlation. However, this is unfeasible, as with this correlation, too much data would be filtered out with the acquired contaminated data at the facilities of the NIOZ. In most cases when applying the suggested filter thresholds, more than 50 % of the data will be filtered out, with extremes of over 90 % being filtered out. However, when implementing this threshold for some data sets 5 % of the data will be kept. Logically, having this amount of data will not be sufficient to do a 12-point polynomial interpolation in between the good data points.

Despiking is done in the MAJ's Velocity Signal Analyser (VSA), software (Jesson et al., 2015). After applying filter thresholds, a software 12-point polynomial interpolation the best-fit polynomial through valid data points, next to the spikes, is calculated and replaces the interpolated value (Goring & Nikora, 2002). Within the VSA software, these thresholds can be altered to get the desired outcome. The various thresholds applied within this software are used to get the best fit for the cascade of energy within a water flow.

What is needed for the spectral analysis to work is sufficient despiking within the limits of the data quality. Three things will be evaluated in the following paragraph, effects of filtering data, and selecting filter threshold despiking.

4.1.1 Effect of Despiking Data

Capturing the instantaneous velocity of water is needed to determine the behaviour of water flow, an ADV can be used for this. Logically, measurement errors will be present when recording the movement of this water flow. These measurement errors need to be

mitigated to show the trends. In Figure 14, the various recordings are shown, random white noise, an unfiltered recording from the experiment, and a filtered recording from the experiment. The -5/3 law shows the natural decay of turbulence. The recording is an example to show the effect of despiking of data, with different filter thresholds, on the change within the power spectral density analysis.

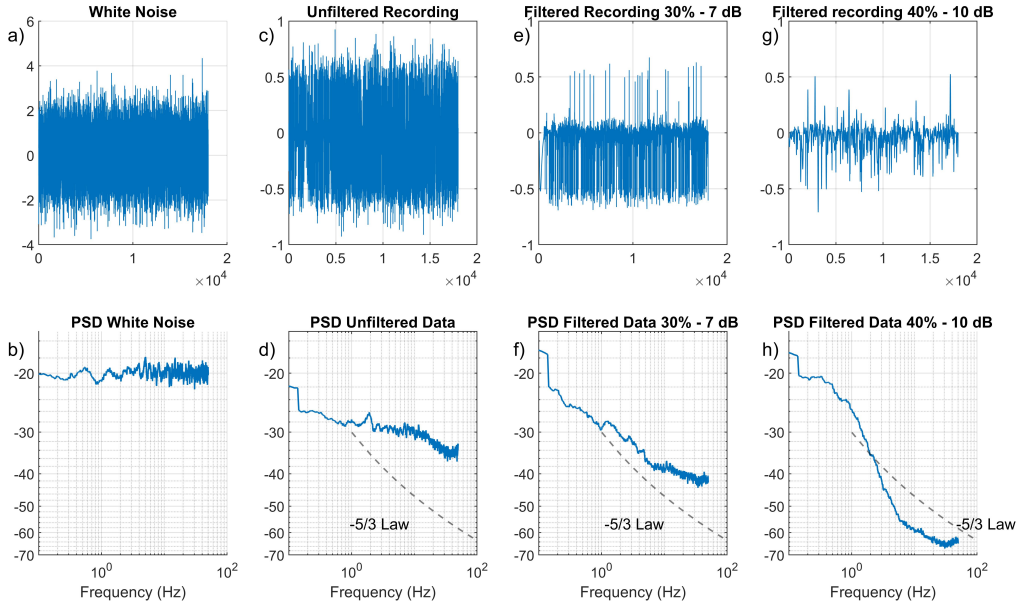

Figure 14: Effect of recording and filters on white noise and power spectral density (PSD) analysis. In **a** and **b** respectively, a white noise signal and power spectral analysis of the white noise are shown. In **c** and **d**, the same is shown for an unfiltered recording of a water flow. Again, the same is shown in **e** and **f**, but for the filtered data with a 30% correlation - 7 dB filter threshold before despiking was done. Lastly, the same is shown in **g** and **h**, but for the filtered data with a 40% correlation - 10 dB filter threshold. The dashed line represents the -5/3 law, the natural dissipation of turbulence.

.

When there is a random signal, white noise, it can be seen that the power spectral density analysis does not decay when the frequency increases, as seen in Figure 14 **b**. This implies no cascade of energy within the data. A raw recording of a water flow, seen in Figure 14 **c**, has considerable amout of noise in it. The power spectral analysis of the unfiltered data in Figure 14 **d**, shows decay closer to the -5/3 law compared to the white noise in Figure 14 **b**. When the data is despiked with a filter threshold, there is still noise in the recording, but the overall trends become apparent. This is shown in the subfigures **e** up to **h**, where the cascade of energy of the despiked data is greater compared to unfiltered data. However, sub-figure **h** shows too great of a cascade of energy when applying a 40% correlation - 10 dB filter threshold before despiking for the example data. This too great of a filter threshold takes out too many small fluctuations making the despiked data not represent the natural decay of energy.

The power spectral analysis of the filtered data shows the necessity of filtering data to be able to have data that takes out unwanted noise and irrelevant components. These errors in the recording are called noise. Engineers regard white noise as a random process around a mean (Kuo, 2018). The signal of white noise is random, therefore the spectral density function will be constant (Kuo, 2018). This constant spectral density analysis can be problematic when analyzing flow behaviour as no decay of energy is present. As a

result, this can make the amount of fluctuation too great which makes TKE, for example, very large. By applying sufficient filter thresholds before 12-point polynomial interpolation, the cascade of energy determined by Kolmogorov (1941a) can be approached.

The power spectral analysis can confirm the presence of Von Karman vortex streets when positioned in the location of greater turbulence intensity in transverse flow direction (Liu et al., 2018). The authors explain how a distinct peak in the power spectral analysis indicates this. A larger peak indicates a more powerful Von Karman vortex street. This peak cannot be seen within the example data of Figure 14 as this is not located at the required location within the wake of the patch.

When sufficiently applying filtering thresholds, the misinterpretation and inaccuracies of the assessment of the underlying frequencies will be enhanced. The filtering will need to be done within the boundaries of the quality of the data. By doing so, the best possible analysis within the limitations of the data can be done. In the next section, the filtering threshold best suited for the data quality will be selected.

4.1.2 Results Despiking Data

What is needed for the analysis of flow-vegatation feedback analysis is sufficient despiking. When too much white noise is present, the power spectral analysis will be constant and no decay of energy will be present, as explained in the previous section. Getting the filter thresholds to be able to take out white noise and approach the -5/3 law decay of turbulence is required. Below, the analysis of the filtering will be shown to give insight into the behaviour of the data on various filters. This despiking has been done for both the emergent and the submerged patch configurations. Respectively, an explanation will be given for each analysis.

For the power spectral analysis, the location on the center line of the patch with maximum transverse turbulence intensity is taken, just like Kitsikoudis et al. (2020) did in their experiments. Between the two data sets, the emergent configuration recording is of greater quality than the submerged configuration recording. This will become more apparent in the next subsections, where the longitudinal and transversal profiles are evaluated.

Filter Thresholds When despiking data, filter thresholds are applied to determine which data points are valid. Thereafter, a 12-point interpolation is done between the valid points. To become familiar with the data first an analysis will be done on how many data points are valid for the different datasets using different filter thresholds, below this will be elaborated.

Three data sets measure the behaviour of each configuration due to the limitations of the measuring setup elaborated in the methodology. When measuring the flow, each dataset measures 60 cm of flume, while 156 cm of flume needs to be evaluated. Therefore, three datasets are needed for each configuration. Within the emergent configuration from upstream to downstream, the test numbers are, subsequently, E1, E2, and E3. For the submerged case, it is S1, S2, and S3 respectively. The percentages of data points above the various filter thresholds are shown in Appendix A in Table 5, 6, and 7. Additionally, the specific test numbers are shown within these tables. The filter thresholds consist of two parameters correlation percentage and signal-to-noise ratio (SNR). As an example, filter threshold 10% correlation and 3 dB SNR is indicated as 10-3.

For the emergent data recordings, u and w velocities were better performing compared

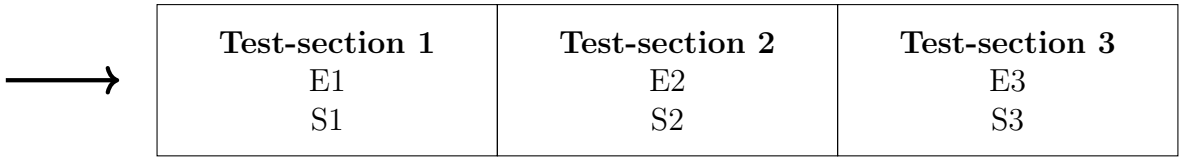

Figure 15: Test sections with the various recording labels. Emergent configuration is labelled with **E**. Submerged configuration recordings are labelled with a **S**. The direction of flow is indicated by the arrow.

to the u velocities recording. For the lower correlation-SNR thresholds, 10-3 and 15-4, the percentage of the data points above the threshold is above 90%. When applying higher thresholds 30-7 and 40-10, this percentage drops to approximately 65% and 40% respectively. In the w direction, these percentages are slightly lower with the lower thresholds all being above approximately 80% of the data points exceeding the thresholds. Logically, the higher thresholds have a smaller amount of data points reaching over the threshold. The lowest-performing axis measured, the u direction, has a percentage of data exceeding the lower thresholds of approximately 65% and 45%. The higher threshold of 40-10 goes below the 6% of the data being sufficient in the emergent configuration data sets.

On the other hand, the submerged configuration recording is of lesser quality, as fewer data points are valid compared to the emergent data sets with the same filter threshold. The downstream recordings, S2 and S3, perform slightly below the emergent dataset recordings, E1 up to E3. The recording closest to the patch, S1, performs below the trend of the other recordings. In the u velocities, the percentage exceeding the threshold for the lower thresholds on the downstream recording for the lower thresholds is above approximately 88%, 32%. and 78% respectively for u, v, and w direction. For the S1 dataset, closest to the submerged patch, these percentages respectively are 69%, 26%, and 50%. For the highest threshold, 40-10, the percentage is even lower than the emergent case making these filtered data logs unusable.

Comparing the emergent and submerged configurations, the submerged data recordings have lower data quality. Especially the recordings closest to the patches, S1, where the most detail is required, are of lower quality compared to the other recordings. Therefore, the peaks in the power spectral analysis of the emergent configuration's recording will be easier to distinguish as the data is of greater quality.

Power Spectral Density Analysis The decay of turbulence can be analyzed using a power spectral density analysis. This can be done anywhere within a flow. However, to be able to distinguish the power of a Von Karman vortex street it is required to it at the location on the centreline behind the patch at which the transverse turbulence intensity is the greatest. The transverse peak in turbulence intensity shows the start of the Von Karman vortex street, as this is where the shear layers join each other again (Kitsikoudis et al., 2020). The power of the Von Karman vortex will be determined in section 4.2.1. Therefore, it has been chosen a location at this point within the flow so that the power spectral density analysis will only need to be done at one location for both analyses.

The locations at which the power spectral density analysis has been done, has been determined with the use of existing literature in combination with the longitudinal profiles shown in the next section. The lower data recording of the submerged configuration, especially close to the patch for the submerged configuration, the experiments of Liu et al. (2018) show how the length of the steady wake region and the start of the Von Karman

vortex street become about half the length for a fully submerged case compared to an emergent case. In the authors' experiments, with a solid volume fraction (ϕ) of 0.15 and diameter of 7 cm the length at which the Von Karman vortex street started was $17 \pm 3cm$ and $7.7 \pm 1.9cm$, respectively, emergent and submerged. The solid volume fraction is compatible with the one used in the conducted experiments, $\phi = 0.149$. Therefore, half the distance behind the patch will be taken for the fully submerged cases. The next measured location closer to the patch will also be analyzed to account for the staggered configuration's shortened steady wake region of the upstream patch, as demonstrated in the experiments of Kitsikoudis et al. (2020).

For the emergent configuration, four locations have been considered for the power spectral density analysis, shown in Figure 16 by the red markers. For the downstream patch, the transversal peak is situated at approximately $6D$ or $7D$ behind the patch. The analyses for the upstream patch have been done $5D$ and $6D$ behind the patch due to the shortening of the steady wake region.

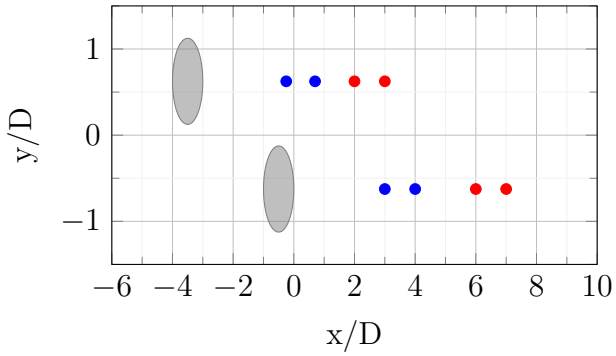

Figure 16: Locations power spectral density analysis for emergent and submerged configurations at which transverse turbulence intensity was the greatest. Respectively, indicated by red and blue markers.

The submerged patches have a shorter steady wake region due to the vertical vortex present as flow migrates over top of the patch. Therefore, the location of transverse turbulence intensity is situated closer to the patch. As explained above the distance of this location is about half compared to the emergent configuration. Therefore, for the upstream patch respectively, 2.75 and $3.7D$ behind the patch have been chosen for the spectral analyses. Additionally, for the downstream patch, $3D$ and $4D$ have been analyzed. In Figure 16 these locations are indicated by the blue markers.

Power Spectral Density Analysis Emergent Configuration The power spectral analyses of the various coordinates indicate that some filters leave too much noise and others take out the underlying patterns. In Figure 17, it can be seen that the 10% correlation and 3 dB filter, for the downstream patch, is too low of a filter, as the power spectral analyses show an analysis approaching a horizontal line. This is an indication of too much white noise. For the analysis of the center line of the upstream patch, this filter performs better as it is close to the -5/3 law line. For all cases, the higher filters, 40 correlation - 10 dB and 30 correlation - 7 dB, the threshold is too high for the quality of the data, as the cascade of turbulence is too great in Figure 17. The 20 correlation - 5 dB filter performs well on the downstream patch's centre line. Overall, the 15 correlation - 4 dB filter performs the best overall, as the -5/3 law reference line fits this depiked data best. The 20 correlation - 4 dB threshold has too great of a decay of turbulence in the

upstream patch's analysis. This can, in part, compromise the analysis of the profiles in the next sections.

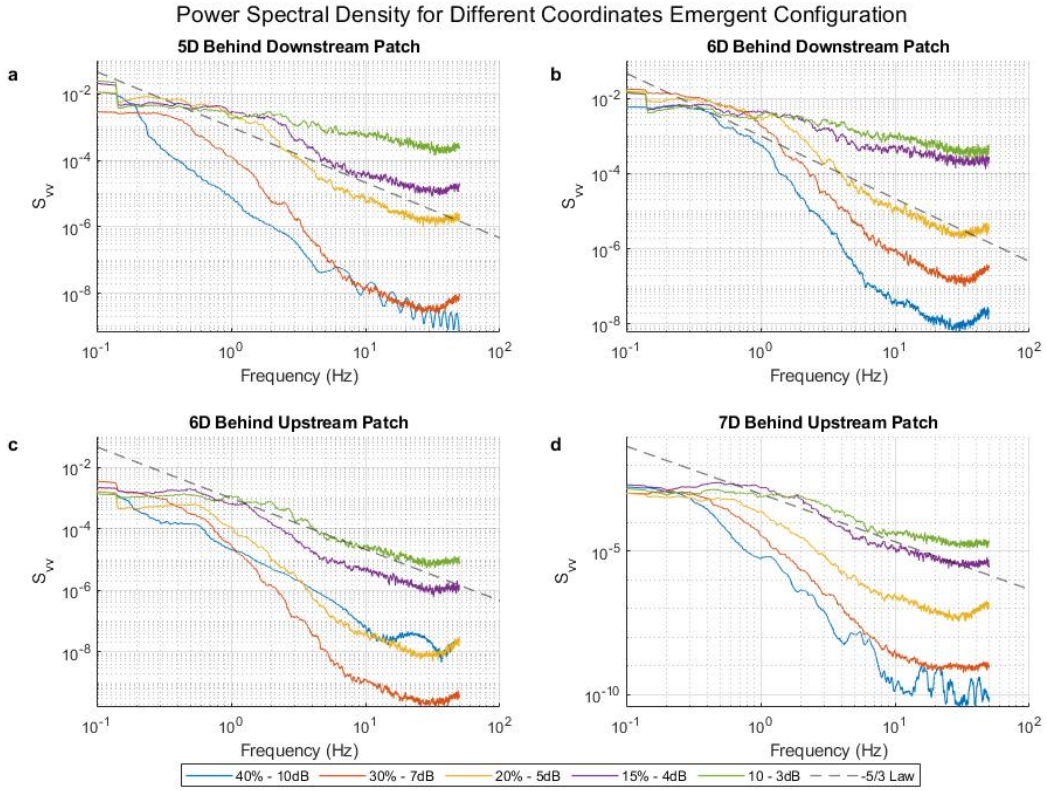

Figure 17: Power spectral densities with various filter thresholds despiking for emergent patches for velocity v. The filters affect how the decay of turbulence will be present in the filtered data set. **a** and **b** show power spectral density behind the downstream patch's center line. **c** and **d** show the density behind the upstream patch's center line. The legend shows the various filters applied and, additionally, the 5/3 law of dissipation of the turbulence line.

Power Spectral Analysis Submerged Configuration For the fully submerged configuration, data recordings at the estimated turbulence intensity peak location downstream from the up and downstream patches show that the data is of overall lower quality compared to the emergent case. This can be seen by the $2.75D$ behind the upstream patch's downstream edge, in sub-figure c of Figure 18. The data does not show a natural decay anymore for the 20 correlation 5 dB thresholds. This 5/3 law decay is better represented in the 15 correlation 4 dB threshold spectral analysis lines in sub-figure c. Again, the lowest thresholds have the most horizontal nature due to the most noise being kept compared to the other thresholds applied. The 40 correlation - 10 dB and 30 correlation - 7 dB thresholds, again, are too high a threshold for the quality of the data recordings. Applying the 20 correlation - 5 dB threshold is not problematic for sub-figures a, b, and d and shows a little too sharp of turbulence decay.

Selected Despiking Threshold In Figures 17 and 18, the effect of the filters on the dissipation of turbulence is seen. The recorded Acoustic Doppler Velocimetry data, crucial for understanding the behaviour of water flow, is of very low quality. The filter of 70% correlation and 15 dB SNR, suggested by Nortek Group (2022), cannot be applied

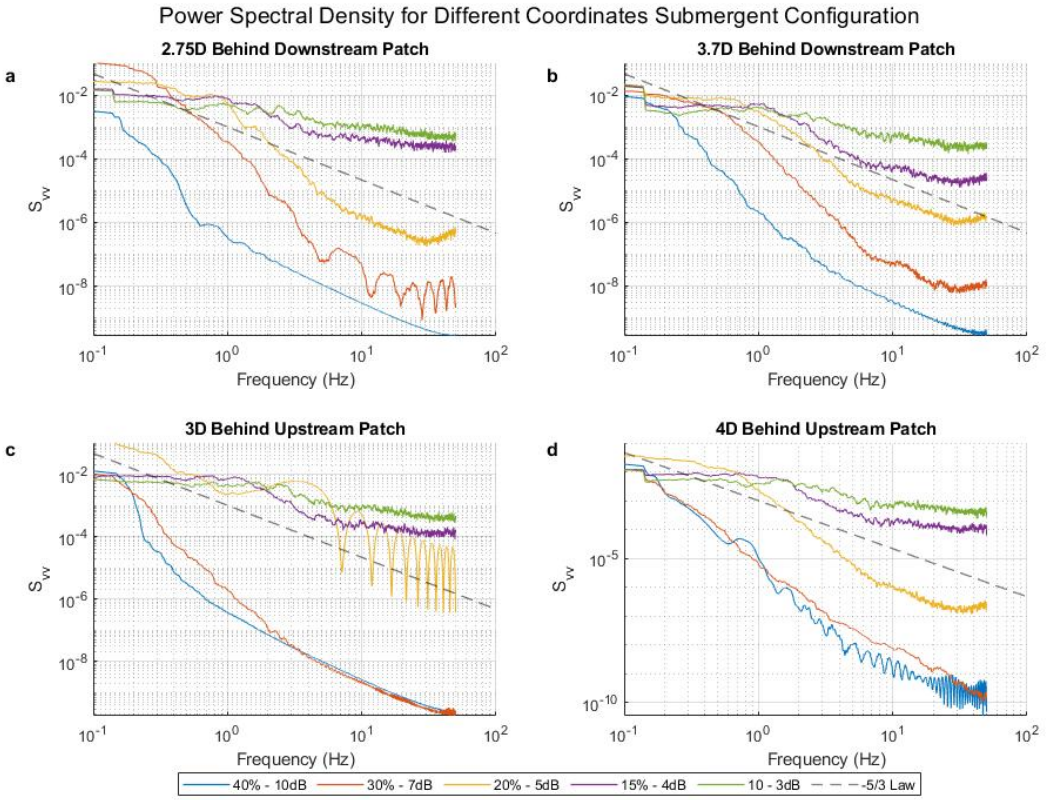

Figure 18: Power spectral densities with various filter thresholds despiking for submerged patches for velocity v. The filters affect how the decay of turbulence will be present in the filtered data set. **a** and **b** show power spectral density behind the downstream patch's center line. **c** and **d** show the density behind the upstream patch's center line. The legend shows the various filters applied and, additionally, the 5/3 law of dissipation of the turbulence line.

to the data. The noise, of which too much is present for the filter thresholds within the data, would surpass the allowable thresholds and not reflect the reality of the water flow behaviour. Additionally, when exceeding this threshold even more, the interpolation between valid data points will become very long and also not reflect reality. When the filter is too high, the fluctuations will not be from the recording but from the interpolation applied; this is already seen in Figure 18. Considering this behaviour to the applied filters, it is sensible to apply the 15 correlation - 4 dB threshold to the data for further analysis of the flow behaviour.

Overall, between the two staggered configurations, applying a 15% correlation 4 dB SNR threshold to the data is the best filter considering the quality of the data. Using this threshold with the 12-point polynomial interpolation between the valid data points will give the result closest to the -5/3 law. Additionally, especially the u and w velocities, approximately over 80% of the data points are valid, except for the 00036 recording. Therefore, with the analyzed filter thresholds, the natural decay of turbulence is approached the closest with the 15% correlation 4 dB SNR filter.

4.2 Flow in the wake of patches, emergent versus fully submerged

This section aims to answer sub-research questions 2 and 3. Three perspectives will be given to determine the difference in flow behaviour between emergent and submerged patches in a staggered configuration. First, the power spectral density analysis of the selected filter threshold will be compared for the upstream and downstream patches. After that, the longitudinal profiles will be examined. Lastly, the transverse profiles will be analyzed. The selected filter threshold of 15% correlation and 4 dB SNR has been used in the analysis within this section for the newly collected data. The reference data logically does not have these filter thresholds before despiking as the data is of greater quality.

4.2.1 Power Von Karman Vortex Street

Using the power spectral density analysis, the significance of the Von Karman vortex street can be observed. This significance of the Von Karman vortex street implies how powerful it is. A more powerful Von Karman vortex street will have a greater amplitude of the oscillating motion within the flow. Therefore, when more flow is diverted, this amplitude, and therefore the total transverse width of the Von Karman vortex street, will be greater. When more flow is diverted the 'peak' in the power spectral analysis will be greater as the amplitude is greater. This is shown by (Liu et al., 2018) where emergent patches have a greater peak in their power spectral density analysis compared to submerged patches.

The shedding frequency around a solid cylinder can be determined using the Strouhal number, defined as $S_t = f_D D/U_0$, where f_D is the shedding frequency. For a solid cylinder of 7 cm with a U_0 of 14 cm/s the cylinder Reynolds number is $Re_D = U_0 D/\nu = 9761$. This cylinder Reynolds number corresponds with a Strouhal number, f_D, of 0.2. The shedding frequency of a solid cylinder of 7 cm in a flow of 14 cm/s is therefore, the shedding frequency, $S_t =$, is 0.1 Hz. In the experiments of (Kitsikoudis et al., 2020) this calculated shedding frequency of the solid cylinder also agreed with the medium patch. The model patches used by (Liu et al., 2018) had a shedding frequency between 0.08 and 0.12 Hz.

For the emergent patch configuration, the power spectral density analyses comparison can be seen in Figure 19. There is no peak observed like in the literature, likely due to the noise still present in the data. However, the red line of the upstream patch does show an increase in power density, after a dip, up to approximately 0.4 Hz and 1 Hz, respectively 5D and 6D behind the patch. This increase in power is less apparent for the downstream patch. What is apparent is that the downstream patch has a greater power density of the frequencies behind the downstream patch compared to the upstream patch. This suggests that the upstream patch's Von Karman vortex street is distorted due to the jet flow between the patches. The shedding frequency is however not the same as calculated for a solid cylinder.

For the submerged patch configuration, peaks in the power spectral analysis show similar decay in energy compared to the emergent patch configuration, shown in Figure 20. However, the profiles of the upstream and downstream power spectral density analysis are very similar. Due to the fully submerged configuration, this is likely due to the vertical vortex. This vertical vortex causes the behaviour behind the staggered submerged patches to be the same. Therefore the jet flow in between the submerged patches does not seem

to influence the upstream patch's steady wake region. Again, it can be said the shedding frequency is not the same as a solid cylinder.

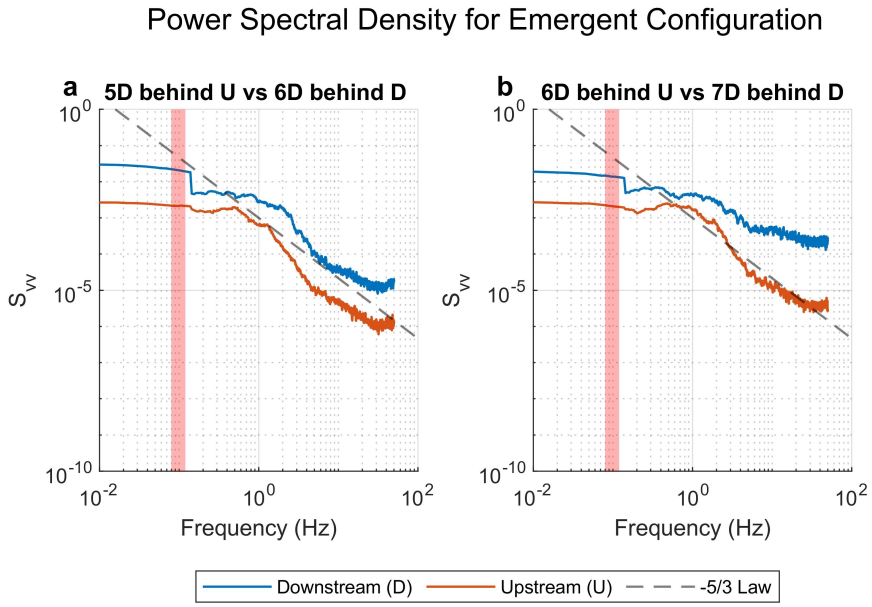

Figure 19: Comparison upstream and downstream patches power spectral density analysis for emergent patches. Respectively, indicated by red and blue lines. The red region shows the range in which vortex shedding would occur for solid cylinders. The vortex shedding would be indicated by a peak in the power spectral density within this region.

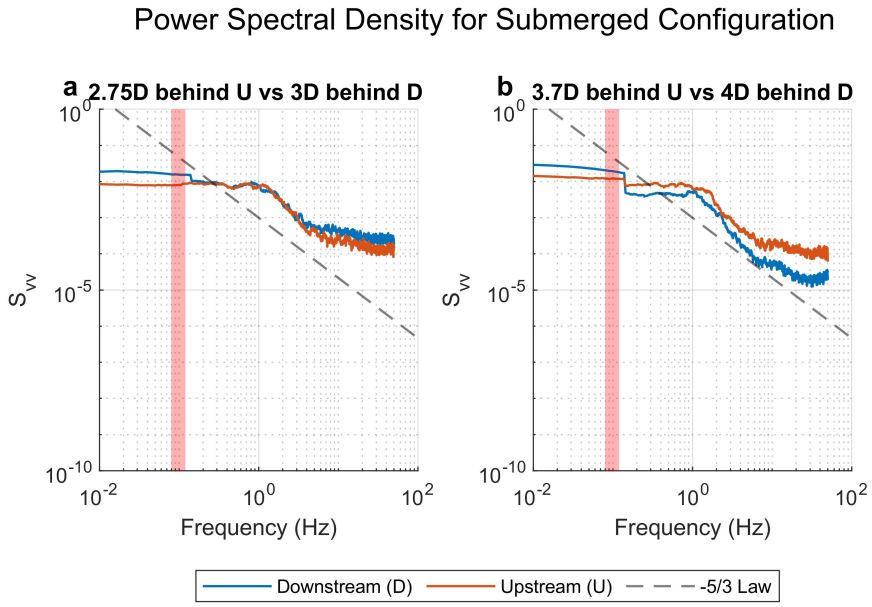

Figure 20: Comparison upstream and downstream patches power spectral density analysis for submerged patches. Respectively, indicated by red and blue lines. The red region shows the range in which vortex shedding would occur for solid cylinders. The vortex shedding would be indicated by a peak in the power spectral density within this region.

4.2.2 Longitudinal Profile Analysis

Using longitudinal profiles along three centrelines will give insight in different flow behaviours on different locations within space relative to the downstream patches edge, $0D$. The three locations are on the centreline of the downstream patch, between the patches, and of the upstream patch. Each location will have the normalized time-averaged velocity, normalized TKE, and normalized transverse turbulence intensity. In this section, the results of both the emergent and submerged patch configurations will be compared with the pre-existing, reference, data provided by Kitsikoudis et al. (2020). The reference data uses two cases, medium and dense, staggered configurations. What needs to be noted is that the reference data does not have the same transversal and longitudinal spacing, and the solid volume fraction differs, as also mentioned in the methodology.

Emergent Longitudinal Profile Analysis To determine the behaviour of the emergent longitudinal velocity, TKE profiles, and turbulence intensity in the transverse direction in Figure 21 show different components of the behaviour of the water flow, indicated by the red markers and making use of the left y-axis. The reference data of Kitsikoudis et al. (2020) helps to be able to compare the data recording's behaviour. The reference data uses two cases, medium and dense, staggered configurations. Respectively, these use the green and beige markers and both use the right axis.

The velocity on the three longitudinal profiles, all on centerlines, will be evaluated behind the upstream patch, between the patches, and behind the downstream patch. In both cases, the flow velocity drops, as the mean normalized flow velocity $\overline{u}/U_0 = 0$ for the incoming flow velocity behind the patch, as seen in sub-figures **a** and **g**. Moving further downstream from the rear edge of the patches, it can be observed that the velocity increases again. This behaviour is comparable with the reference data shown in green and beige. In sub-figure **a**, the downstream patch, a peak in velocity is hard to distinguish, as the normalized velocity of emergent configuration's data is very scattered. Solely, the overall trend suggests that behaviour is comparable with the reference data. The profile of the emergent case, sub-figure **g**, behind the upstream patch, shows the peak velocity slightly sooner compared to the reference data. A peak velocity for the emergent configuration can be noticed at $4.4D$ behind the upstream patch, $1.3D$ relative to the downstream patch. This however is logical as the patches are longitudinal closer to each other. The jet flow between these patches will be greater causing the steady wake region to shorten, and therefore reaching this peak velocity sooner. The measurements in sub-figure **g** suggest no recirculation of flow is present behind the emergent upstream patch as no negative normalized average velocity is observed. Re-circulation cannot be seen on the upstream patch's centerline of the reference data, as measurements could not be taken further upstream. However, on the downstream patch, the reference date shows how the flow initially recirculates before gaining velocity again. The denser patch of the reference data has greater recirculation as more flow is diverted around the patch.

The TKE energy profiles for the staggered emergent configurations are shown in Figure 21 **b**, **e**, and **h**. The turbulence kinetic energy is much greater compared to the reference data. Especially the downstream TKE is a magnitude greater compared to the reference data. This is likely due to the contaminated data which still has noise in it causing the TKE to be greater. The peak in TKE behind the downstream patch occurs slightly later compared to the reference data configurations. The difference in transverse and longitudinal positioning compared to the reference data's case is likely the reason.

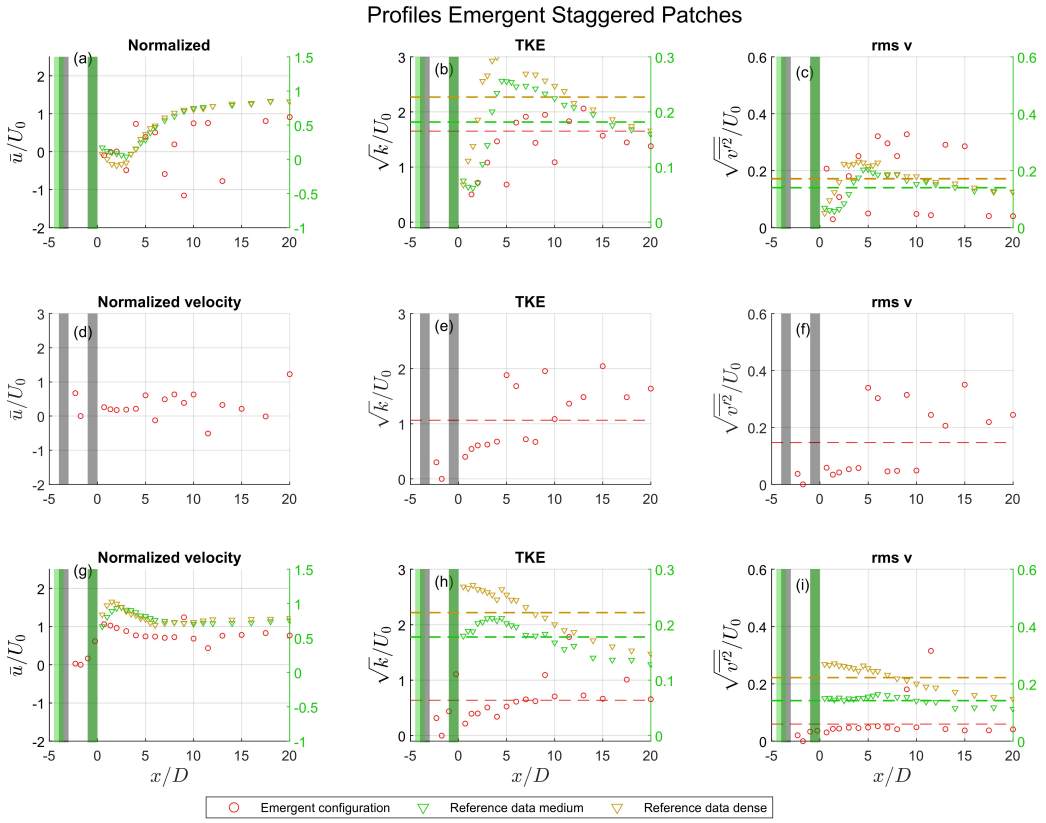

Figure 21: Profiles for three transversal location of emergent configuration: center-line behind upstream, center-line between patches, and center-line behind downstream patch. The normalized mean longitudinal velocity, $\overline{u}/U_0$, profiles are shown in subfigures **a**, **d**, and **g**. Normalized Turbulent Kinetic Energy (TKE) longitudinal profiles are shown in subfigures **b**, **e**, and **h**. Lastly, the remaining sub-figures show normalized square-root turbulent kinetic energy, $\sqrt{k}/U_0$, in sub-figures **c**, **f**, and **i**. Reference study data is plotted of medium and dense patches spaced longitudinally $2.5D$ and transversely $0.5D$, indicated by green bars. The longitudinal patch positions of the experiments conducted are indicated by grey bars.

What is shown by the reference data is that greater diversion of flow, due to a greater ϕ, results in greater TKE. The profile behind the upstream patch, sub-figure **h**, does not show a distinct peak like the reference data does. The red markers in sub-figure **h** however do plateau after increasing up to approximately $7D$ relative to the downstream edge of the downstream patch. This is interesting as TKE should decrease moving further away from the patch. Comparing the TKE between the upstream and downstream patch profiles it is apparent that the upstream patch has much lower TKE. Between the patches, sub-figure **e**, the TKE trend suggests that the jet flow adds turbulence to the flow between $6D$ and $10D$, Initially, the flow is low in TKE as no diversion of the flow between the patches is present.

The turbulence intensity in the transversal direction is more substantial in the downstream patches compared to the upstream patch for the emergent configurations, when comparing sub-figure **c** and **i**. This is remarkable, as the jet flow between the patches would make the turbulence intensity behind the upstream patch greater. This increase in turbulence intensity can be seen between the patches, sub-figure **f**. Again this suggests a jet flow between the patches. The turbulence intensity behind the downstream patch is much more scattered compared to the upstream patch. For both cases, it can be seen the is an increase in transverse turbulence when moving away from the downstream edge.

When the two shear layers start interacting the peak transverse turbulence intensity is seen. Where after, the transverse turbulence intensity drops again. This drop is however not seen in the overall trend between the patches in sub-figure **f**.

Submerged Longitudinal Profile Analysis Behind the submerged patches, the same three longitudinal profiles have been made as behind the emergent patches. In Figure 22 these profiles can be seen. Again the same reference data with the emergent staggered patches from the experiments of Kitsikoudis et al. (2020) have been plotted in the Figure.

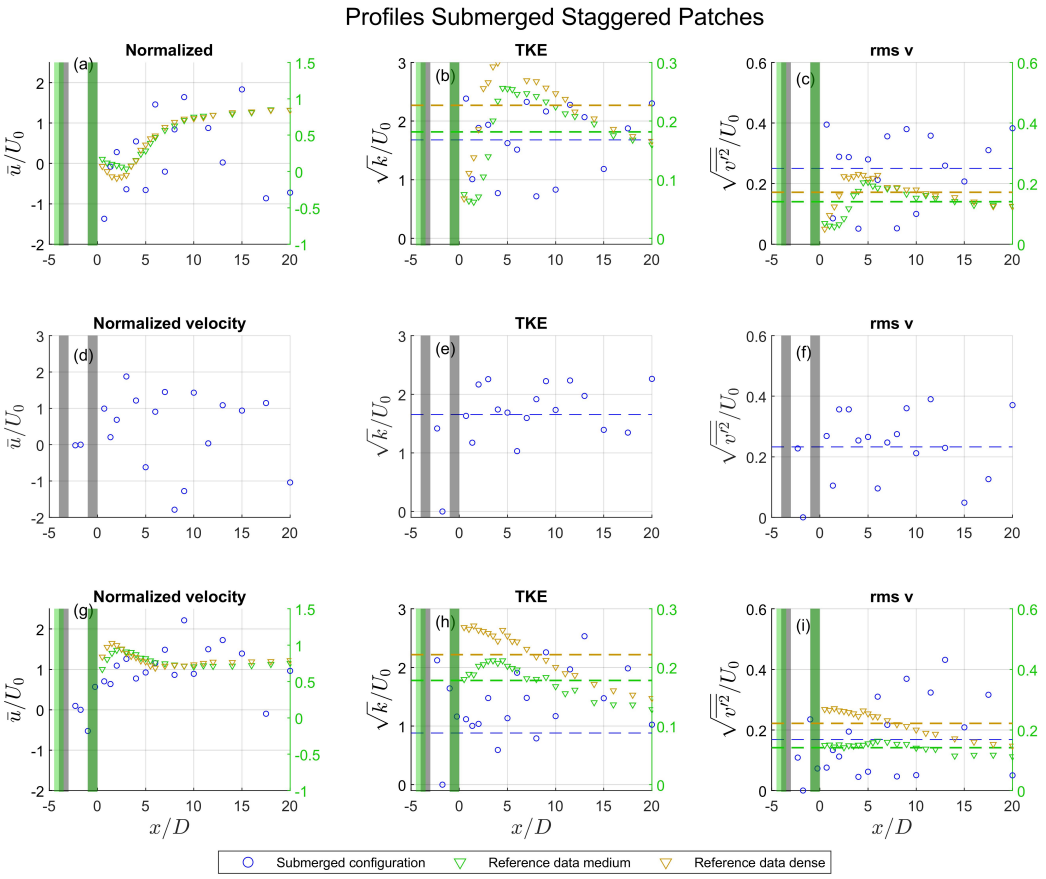

Figure 22: Profiles for three transversal location of emergent configuration: center-line behind upstream, center-line between patches, and center-line behind downstream patch. The normalized mean longitudinal velocity, $\overline{u}/U_0$, profiles are shown in subfigures **a**, **d**, and **g**. Normalized Turbulent Kinetic Energy (TKE) longitudinal profiles are shown in subfigures **b**, **e**, and **h**. Lastly, the remaining sub-figures show normalized square-root turbulent kinetic energy, $\sqrt{k}/U_0$, in sub-figures **c**, **f**, and **i**. Reference study data is plotted of medium and dense patches spaced longitudinally $2.5D$ and transversely $0.5D$, indicated by green bars. The longitudinal patch positions of the experiments conducted are indicated by grey bars.

In the normalized flow velocity longitudinal profiles, sub-figure **a**, **d**, and **g**, scattered profiles can be seen. The downstream normalized flow velocity of the submerged staggered patch configuration has a more scattered nature, this is logical as the amount of data points valid before despiking is approximately 30%. The overall trend for all profiles is that the normalized velocity increases up to a peak, following the main trend of the reference data. Close to the downstream and upstream patches recirculation is observed, which is in line with the literature Liu et al. (2018). Behind both upstream

and downstream patches recirculation is present. Due to the scattered data, it is hard to distinguish how much it exactly is. The velocity between the patches, sub-figure **d**, plateaus at $0.7D$ relative to the downstream edge of the downstream patch where it stays at around a normalized velocity of 1.

The TKE is again an order of magnitude greater compared to the reference data. The average TKE behind the downstream patch centreline is greater compared to the upstream patch as seen in sub-figure **b** and **h**. This is likely due to the additional mixing component, the vertical vortex, behind the downstream patch next to the vertical vortex being present behind the upstream submerged patch. In between the patches, sub-figure **e**, the TKE increases at $2D$ behind the downstream edge of the downstream patch. This is a result of the vertical vortices and the jet flow in between the patches. It is however hard to point out specifics in the behaviour as the TKE results of the submerged staggered patch configuration are so scattered compared to the reference data. The greater TKE solely suggests greater mixing within the flow.

Transverse turbulence intensity results for the submerged is higher on average for the downstream patch compared to the reference data with emergent staggered patch, as seen in sub-figure **c**. In sub-figure **i**, the upstream patch centreline, the submerged patch has greater average transverse turbulence intensity compared to the medium density reference case, but lower than the dense patch density reference case. Solely in the upstream patch a low initial transverse turbulence intensity can be observed where after it increases. The other two cases show a very scattered result.

Comparison Emergent and Submerged Longitudinal Profiles To conclude the results of the longitudinal profiles a comparison between the submerged and emergent staggered patch configurations will be made. Recirculation behind the submerged patches is greater compared to the emergent patches. This greater recirculation as a result of the vertical vortex also causes the TKE to be greater for the submerged patch compared to the emergent patch. The greater transverse turbulence intensity of the submerged patch configuration is remarkable and needs greater investigation. Jet flow between patches for the emergent configuration is expected. Overall, the acquired data has the same trends when compared to the reference data. However, due to the low data quality, patterns are very scattered.

4.2.3 Transverse Profile Analysis

Next to longitudinal profiles, transversal profiles can give a different insight into the behaviour of water flow. Due to time constraints, only specific distances from the transverse profile have been taken. The conducted experiments at the NIOZ and the reference data do not have the same distances relative to the downstream edge of the downstream patch for the transverse profiles. Therefore, first the results of the conducted experiments will be discussed. Thereafter, the results of the reference data and the comparison with patterns with the results of the conducted will be discussed.

Transverse Profile Experiments Normalized flow velocity is shown in sub-figure **a** of Figure 23. The upstream patches, emergent and fully submerged, show similar behaviour. This is especially true for the two transverse profiles at -2.3 and $-1D$. Downstream from the downstream edge, more dissimilarities are shown. At $2D$ below the downstream patch, recirculation can be seen for the submerged patch configuration. Further downstream,

the velocity behind the downstream patch of the submerged configuration increases again, and dictating recirculation is not present anymore. Overall, the fully submerged profile shows greater recirculation compared to the emergent patch. When moving downward from the patch in the longitudinal direction, it becomes apparent that the normalized velocity becomes more uniform in the transverse profile. This can be seen in sub-figure a of Figure 23, where $8D$ behind the patch the velocities start approaching the same velocity. The velocity of $\overline{u}/U_0$ logically becomes 1 when approaching infinity, in the direction of flow, as the velocity restores itself to U_0, for $\overline{u}/U_0$ this would be equal to 1.

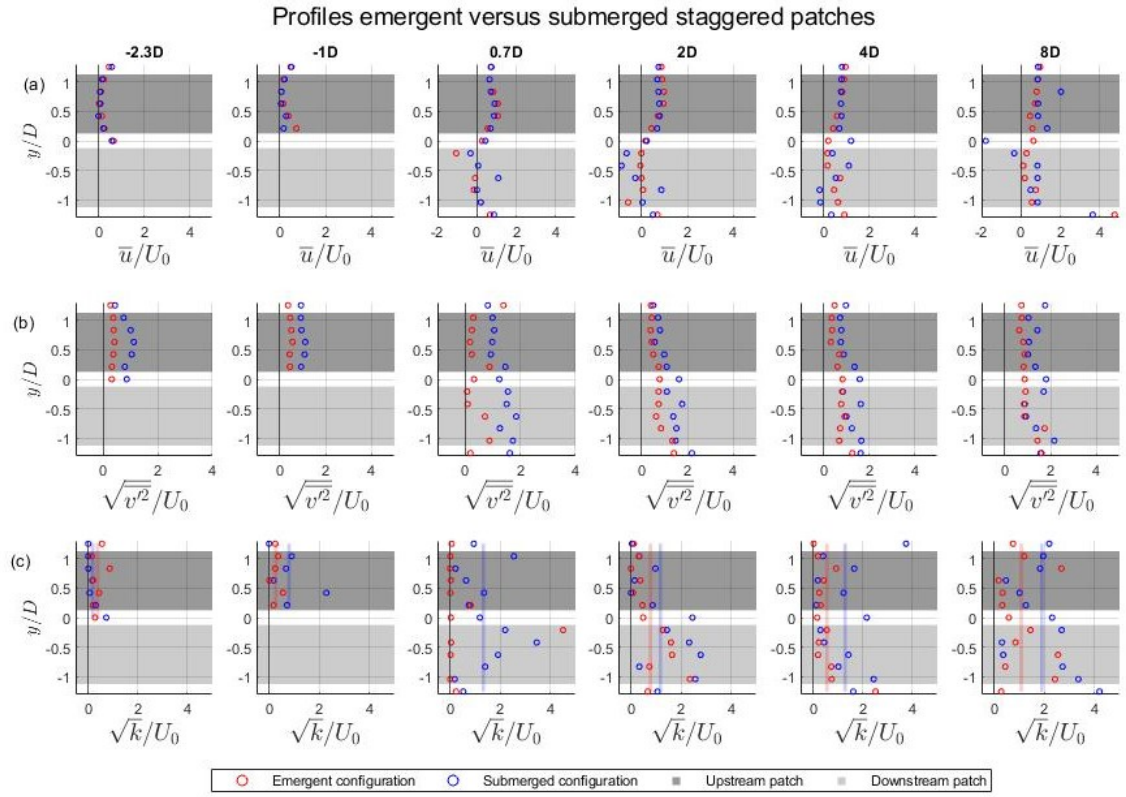

Figure 23: Transversal profiles of normalized **a** mean longitudinal velocity, $\overline{u}/U_0$, **b** transversal turbulence intensity, $\sqrt{\overline{v'^2}}/U_0$, and **c** square root of the turbulence kinetic energy, $\sqrt{k}/U_0$ downstream of emergent and fully submerged staggered patches arrangement. The gray-shaded areas indicate the transversal position of the patches in the unidirectional flow. $0D$ is the rear edge of the downstream patch; dark grey is the upstream patch, and light grey is the downstream patch. Positions are relative to the downstream edge, positioned at 0D of the downstream patch. Negative D positions solely look at the behavior behind the upstream patch. The rear edge of the upstream path is situated at $-3D$.

Figure 23 **b** shows the turbulence intensity in the transverse, v, direction. What is remarkable, as noted in the previous section with the longitudinal profiles, is that the turbulence intensity in the transverse direction is greater with the submerged configuration. A possible explanation is that the recording of the fully submerged configuration is of lesser quality, which leaves more noise in the data. This noise in the transversal axis data translates into higher turbulence intensity. Consequentially, this compromises the results of a sufficient comparison between emergent and submerged configurations in this case. What can be observed is that the emergent case has a more profound steady wake region, as seen at $0.7D$. This can be seen as initially there is low turbulence intensity

TKE, shown in Figure 23 **c**, has shown an obvious difference between emergent and fully submerged patch configurations. The fully submerged patch configuration has a

recirculation zone, as explained in the paragraph discussing Figure 23 **a**. Re-circulation due to the vertical vortex causes greater mixing and, therefore, greater TKE. In all instances, the mean TKE is greater for the submerged case, except for $0.7D$, in which the emergent case has an outlier much greater than the average of the submerged case. What needs to be noted is that the TKE could also be larger since the turbulence intensity in the transverse direction is larger. However, u and w also contribute to the TKE, as seen in the methodology, which is the same portion as v. The TKE of the submerged configuration, nonetheless, is in most instances, as seen in sub-figure **c**, twice as great compared to the emergent configuration. It can be concluded that even with a lower transverse turbulence intensity, the TKE will still be greater for the submerged configuration.

Shear-induced turbulence in water flow can be shown by Reynolds shear stress. When the Reynolds shear stress is high, it indicates a large velocity difference between two layers within a flow. For all plains, the Reynolds shear stress is shown in Figure 24. When Reynolds shear stress is negative, a shear layer is present (Zong & Nepf, 2012). In Figure 24, this shear stress will need to be positive to determine a shear layer, as the negative shear stress is determined.

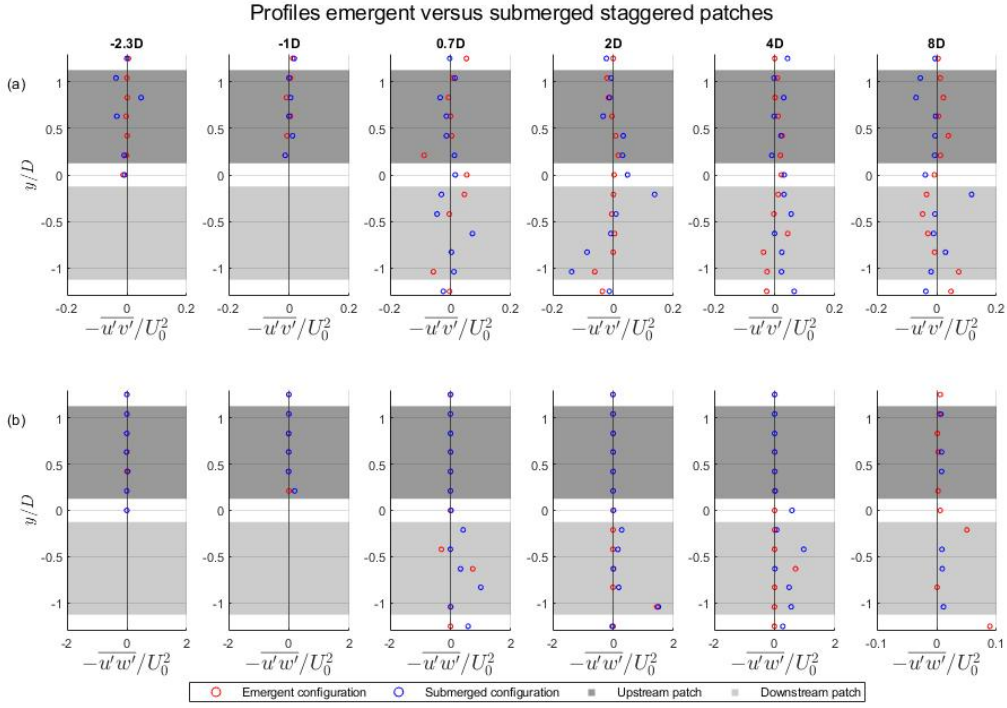

Figure 24: Transversal profiles of normalized, **a**, horizontal Reynolds shear stress, $-\overline{u'v'}/U_0^2$, and **b** vertical longitudinal Reynolds shear stress, $-\overline{u'w'}/U_0^2$ downstream of emergent and fully submerged staggered patches arrangement. The gray-shaded areas indicate the transversal position of the patches in the unidirectional flow. $0D$ is the rear edge of the downstream patch. Negative D positions solely look at the behaviour behind the upstream patch. The upstream path's rear edge is at $-3D$.

What can be seen in Figure 24 **a** is chaotic patterns. The submerged configuration has greater shear stress closer to the patches, it appears. Moving further downstream from the patches at $4D$, these shear stresses are not as present anymore for the submerged configuration. However, clear patterns are not shown, and confident conclusions cannot be drawn for the submerged configuration. On the other hand, the emergent cases show less scattered results. But solely at $8D$ behind the downstream patch, a clear pattern can be seen. The shear layer, at $8D$ shows a jet flow between the two patches. The $-\overline{u'v'}$

is situated close to the centerline of the upstream patch, suggesting a significant jet flow between the patches.

Figure 24 **b** shows greater shear stress, $-\overline{u'w'}$, for the fully submerged configuration. This shear stress suggests a vertical vortex. There is a significant velocity difference between the steady wake region and the velocity of the flow migrating over the top of the patch. Initially, no shear stress in the vertical transversal plane is present as the measurements are done 3 cm above the bed. The patches are emergent and 7 cm within a water depth of 14 cm. The shear stress of the vertical vortex behind the downstream patch can be likely noticed in the $2D$ and $4D$ transverse profiles.

The transverse profiles of the data gathered provide insights into the distinctions between submerged and emergent patches in staggered configurations. Average flow velocities show similar behaviour between the two configurations. Fully submerged patches show greater turbulence and transverse turbulence intensity compared to emergent patches. Reynolds shear stress on the transverse profiles shows limited patterns, which can draw confident conclusions.

Comparison Transverse Profiles with Reference Data The normalized mean velocity transversal profiles for the emergent configuration have similar behaviour to the reference data results shown in Figure 25. What needs to be noted is that the figure of the reference case has more measurements, reaching further outside of the transverse position of the patch. The present experiments only reached one coordinate outside the transverse position of the patches.

The emergent configuration has very similar behaviour to the reference data when looking at the normalized average flow velocity. Both the medium and dense patch configurations in Figure 25 show no recirculation right behind the downstream patch. The normalized average flow velocity is near 0. Within the results of the conducted experiments, Figure 23 **a**, it can be seen there is slight recirculation at $0.7D$ behind the downstream patch for the emergent configuration. This is probably due to the relatively closer transversal position of the emergent patches to one another. In the submerged case the vertical vortex is likely to be dominant in the influence on recirculation. This recirculation is also more dominant compared to the reference cases due to this submergence. Overall the transverse profiles show the same flow behaviour when moving downstream from the patch. For example, the normalized average velocity moves back to $\overline{u}/U_0 = 1$ for both the results and the reference data profiles.

The length of the steady wake region is indicated by the point at which the transverse turbulence intensity is the greatest. The peak transverse turbulence intensity on the centerline behind the upstream patch is observed at $4D$ for the dense-density patch in a staggered configuration, shown in Figure 25. The medium-density upstream patch shows a larger transverse turbulence further downstream on the centreline of the upstream patch, at $10.5D$ behind the patch. The downstream patch in Figure 25 shows the peak transverse turbulence intensity of the dense and the medium-density patch configurations at, respectively, $5D$ and $7D$ behind the downstream edge on the centreline.

For the conducted experiment results these peaks are not as apparent. The maximum on the centreline of the upstream patch for the emergent and the submerged are located, respectively, at -$1D$ and -$2.3D$. For the emergent case, this is much closer to the patch compared to the reference data. The submerged case is logically closer due to the vertical vortex. The downstream patch has the peak transverse turbulence intensity value located on the centreline at $0.7D$ for both submerged and at $4D$ for the emergent. For the

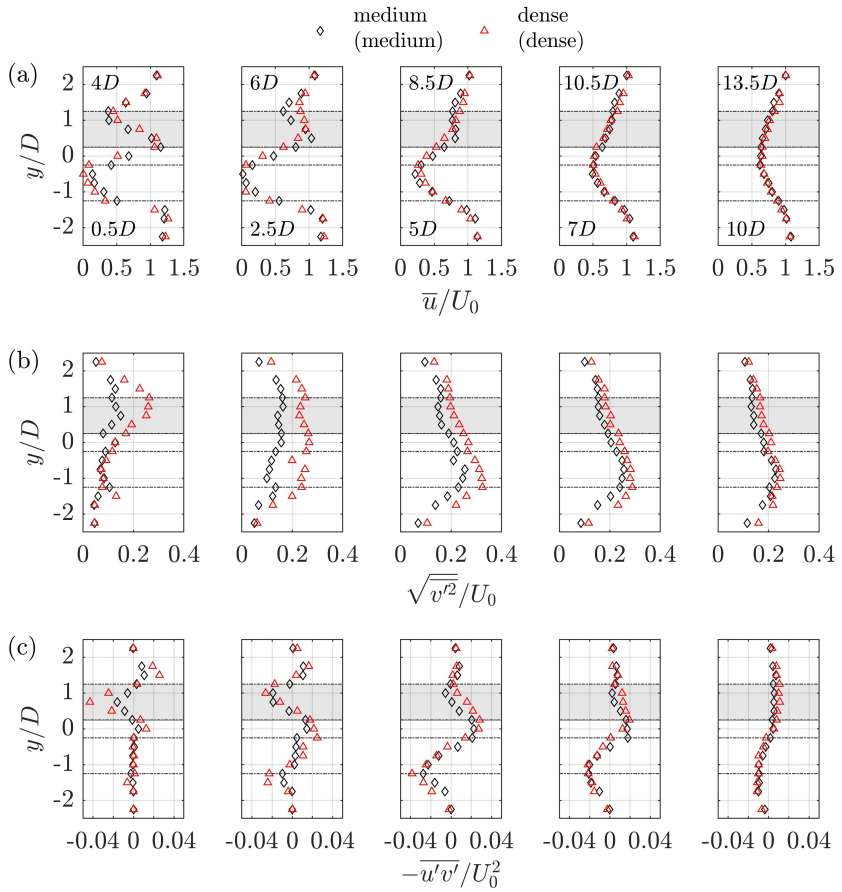

Figure 25: Transversal profiles, of reference data, of normalized **a** mean longitudinal velocity, $\overline{u}/U_0$, **b** transversal turbulence intensity, $\sqrt{\overline{v'^2}}/U_0$, and **c** horizontal Reynolds shear stress, $-\overline{u'v'}/U_0^2$ downstream of the medium and dense patches in staggered configuration. The gray-shaded area bounded by the dashed line indicates the upstream patches transverse position in the uni-directional flow. The dashed line with no shading indicates the transverse position of the downstream patch. $0D$ is the rear edge of the downstream patch. Positions are relative to the downstream edge, positioned at 0D of the downstream patch.

emergent configuration, this shows the upstream patch's steady wake region is shortened. The submerged patch configurations' peak values are so close to each other that it is hard to conclude a difference in steady wake region length.

The horizontal Reynolds shear stress, $\overline{u\prime v\prime}/U_0^2$, shows greater shear for the dense patch configuration compared to the medium-density patch configuration. The greatest horizontal shear stress on the centreline can be observed at $5D$ behind the downstream patch. This shear stress is caused by the jet flow in between the patches. In Figure 24 **a**, solely the $8D$ emergent configuration shows a clear profile of horizontal shear stress. It can be seen the peak horizontal shear stress has shifted towards the centreline of the upstream patch. In the conducted experiments the patches are situated closer to each other transversely and longitudinally. This causes the jet flow to be greater as the flow is 'pinched' more and causes the jet flow to be more powerful in the transverse direction. However, the rest of the profiles are very scattered so this conclusion should be considered of limited value.

5 Discussion

This study has explored the flow-vegetation feedback with patches in staggered configuration, emergent and submerged rigid vegetation, in a unidirectional flow environment. While the study has given insight into the behaviour of staggered submerged vegetation, the study's limitations must be highlighted. By doing so, the implications of these limitations will become clear. The limitations also give future researchers a greater understanding of the conducted experiments. First, the various limitations of this study will be discussed. Thereafter, a comparison with existing literature will be made, along with a deeper analysis of the reference data used in the results.

5.1 Limitations Conducted Experiments

The experiments had several limitations, namely the quality of the results of the ADV sensor, non-constant conditions, developed flow not being present, and patch characteristics. Below these topics will be highlighted.

At the NIOZ facility, the Acoustic Doppler Velocimeter sensor did not perform as needed. Within the laboratory of the institute, there was only one sensor present. Due to the limited time slot within the laboratory, organizing a better-performing sensor was not feasible. Possibly the sensor, used, was broken at the facilities of the NIOZ. The sensor registered a very low correlation and signal-to-noise ratio in the recorded data. The transversal axis sensor was of the lowest quality, which was needed in determining the start of the large-scale mixing and, in part, the Von Karman vortex street. The longitudinal and vertical axes were of greater quality but still not of sufficient quality to be able to apply the filtering thresholds suggested by Nortek Group (2022). Possible improvements can be made in the use of seeding to have enough particles within the flume for the ADV, to reflect its acoustic signals and determine the direction and velocity of the water. However, it is unlikely the amount of suspended particles would be the limiting parameter within the flume setup as the water in the flume was full of algae and sediment, as it was pumped from a reservoir full of water from the Oosterschelde.

As the data is of low quality, it was necessary to have low filter thresholds, as otherwise, too many valid points would be removed and the cascade of energy suggested in the -5/3 law would not be approached anymore. This energy cascade is steeper than the -5/3 law in the filtered data due to the details of small fluctuations being filtered out. The suggested thresholds of 70% correlation and 15 dB SNR by Nortek Group (2022) are not tolerable for the data acquired in this study. When visualizing the velocity over time, it can be observed how the greater filter thresholds too many valid data points get removed and the smaller frequencies in the spectral analysis get lost in the despiking process; these are important in determining TKE as more fluctuations makes greater TKE (Lee & Harsha, 1970). Because of the great amount of contamination in the data, despiked with low filter thresholds for correlation and SNR, the comparison with existing literature is challenging.

The recordings done have resulted in a low-quality data set, especially in the v velocity. For the recording of the submerged patch configuration closest to the patches, S1, two recordings have been done, specifically, 00036 and 00039. Recording 00039 had lower data quality compared to recording 00036. On the other hand, recording 00036 had a smaller water depth compared to all the other recordings, 13.7 cm instead of the required 14 cm. Considering recording 00036 had more valid data points, this record-

ing has been used in the conducted analyses. The smaller the water depth of recording 00036 will influence the results as the flow velocity will be greater compared to the other recordings. This could have negatively influenced the comparison of the emergent and submerged configuration. However, the great difference between the valid data points between emergent and submerged configuration also made this comparison challenging.

To be able to do all the experiments, a platform was made to hold the individual stems. This platform was constructed from a concreteplex plate with holes in the required configuration of the patches. The difference in height between the total depth in the flume and the depth at the measurement was, respectively, 30.5 cm and 14 cm, causing the flow not to be fully developed when coming in contact with the upstream patch because the approach of the concreteplex plates was too short. The flow contraction from the upstream part of the platform to the platform was too great. This could be seen during the experiments by an increase in the water level just past the upstream edge of the platform. In future research, the approach of the platform should be larger to ensure a developed flow. By ensuring this, a better comparison with the existing literature can be made as this will ensure a developed flow.

The experiments conducted solely considered submerged, rigid vegetation patches. However, in ecosystems, submerged vegetation is often flexible, making dynamics even more complex due to the swaying of the vegetation in unidirectional flow. Due to the swaying the width of the patch will become greater as more vegetation is encountered by the flow. Also, flexibility causes the vegetation to be streamlined in the direction of flow and therefore be 'pushed over'. These dynamics are lacking in the experiments performed at the NIOZ. In order for the flow-vegetation feedback in staggered submerged rigid to be thoroughly explored, future research should move towards flexible submerged patches in staggered formations.

The solid volume fractions within the experiments have been kept constant between the upstream and downstream patches. This is a limitation of the study, as this, in nature, is unlikely to occur (Kitsikoudis et al., 2020). In future research, varying upstream and downstream solid volume fractions for submerged staggered patch configuration should be considered. When doing this a connection can be made to the research of Kitsikoudis et al. (2020), where this has been done for emergent patches.

What could also be considered in future research is vegetation in different growth stages in a staggered configuration. Yagci et al. (2024) has explored the flow dynamics of growth stages by defining three stages with emergent patches, each stage adding a patch directly behind the upstream patch. The density of the upstream patch also increases simultaneously when a patch is added downstream. This dynamic could also be explored with height in a staggered configuration. Where the upstream patch has a greater height compared to the downstream height. The height can be increased to simulate growth. By doing this, the dynamic between vertical vortexes of different h/H ratios in staggered configuration can be explored.

In sum, this research was limited by the conditions present at the facilities of the NIOZ. Due to the limited time, only two configurations could have been tested. Also, this caused conditions for the experiments not to be checked before starting experiments, like a developed flow in the flume. A greater amount of configurations would have given a greater understanding of how submergence affects the flow behaviour around staggered submerged patches. Future research should check if the limitations within this research have been avoided before continuing with the start of the experiments.

5.2 Comparing Conducted Experiments

The conducted research has shown its results within the limitations of the facility of the NIOZ. To make a connection with previously conducted research in this section of the discussion a comparison will be made with the existing literature and the provided reference data.

The combination of submerged vegetation and a staggered configuration has not been studied before. Kitsikoudis et al. (2020) and Meire et al. (2014) have studied emergent staggered and side-by-side emergent patch configurations. Submerged isolated patches have been studied by Liu et al. (2018) and Zong and Nepf (2012). The parallels and differences between the new specific conditions studies in this study and existing literature will be denoted below.

Steady Wake Region Length Turbulence intensity in the transverse direction is important in determining where shear layers start interacting and form a Von Karman vortex street. When an emergent patch is present in a unidirectional flow, a greater amount of water is deflected around the patch compared to a submerged patch. Due to this greater amount of water getting deflected, the peak transverse turbulence intensity should be greater for an emergent patch (Kitsikoudis et al., 2020; Liu et al., 2018). When more movement is present in the transverse direction, the turbulence intensity should also be greater in this direction. In the conducted experiments, the turbulence intensity in the v direction is greater for the submerged configuration compared to the emergent configuration; this result is counter intuitive. Most likely, this is caused by the quality difference of the data. The greater contamination within the submerged configuration's dataset is likely the cause of the increased turbulence intensity. These analyzed results of the submerged patch configuration do not show higher observed turbulence but rather a great variance in outliers. This variance causes this greater transverse turbulence intensity to be present in the results.

Liu et al. (2018) has shown in their study how decreasing the ratio from $h/H = 1.0$ (emergent) to $h/H = 0.5$ will result in a shortening of the steady wake region from 17 cm to 7.7 cm for an isolated patch. The peak transverse turbulence intensity of the downstream patch for the emergent configuration in this study was found at approximately $6D$ behind the downstream edge, as seen in Figure 21. The peak transverse turbulence intensity is hard to distinguish in Figure 23. The peak transverse turbulence intensity on the centerline behind the upstream patch is observed at $4D$ for the dense staggered configuration, shown in Figure 25. Considering the shorter steady wake region, when looking at the peak transverse turbulence intensity in Figure 21, within the conducted experiments of emergent patch configuration, a slightly shorter distance was observed compared to the downstream patch. This shortening is also observed by Kitsikoudis et al. (2020), where a significant shortening of the upstream patches' steady wake region occurred due to the presence of the downstream patch.

Meire et al. (2014) showed in their experiments how neighbouring emergent patches will start behaving as one single body bluff when close enough to each other. The transversal closer positioning of the patches might affect the recirculation behind the downstream emergent patch. It is unlikely the two patches will behave as one bluff body. Meire et al. (2014) pointed out with side-by-side patches the separation distance needs to be above 10-20% to behave as a single bluff body. The transverse distance of $0.25D$, in the conducted experiments in this study, in combination with the longitudinal spacing, will make the

two patches in staggered configuration behaving as one bluff body unlikely. Therefore, separate Von Karman vortex streets are still possible in the transverse closer position compared to the experiments done by Kitsikoudis et al. (2020). These patches logically both therefore have their own steady wake region.

Normalized Flow Velocity For the submerged patch configuration, it can be observed in Figure 23 **a** that the recirculation and mixing are much greater compared to the emergent configuration for the downstream patch. Zong and Nepf (2012) determined that with patches denser, than $\phi = 0.10$ recirculation will be present. The experiments conducted, therefore, correspond to the research done by Zong and Nepf (2012), where $\phi = 0.15$ is used. Additionally, (Sadeque et al., 2008) also found greater recirculation behind isolated submerged patches compared to emergent patches. Behind the upstream patch at $-1D$ and $-2.3D$, there is no significant difference between the emergent and submerged configurations, as seen in Figure 21 and 22. The upstream patch is likely affected by the jet flow in between the patches. This, however, will need further research to be certain the jet flow affects the upstream patches recirculation. Especially because the power spectral density analysis shows the same profile for the up and downstream submerged patches, indicating identical turbulence decay. This in part suggests the same flow behaviour elements being dominant in the decay of frequency, this will be elaborated on in the paragraph Power Spectral Density Analysis below in subsection 5.2.

Turbulent Kinitic Energy In the longitudinal results, shown in Figure 21 and 22, it becomes apparent the conclusions of the data of the conducted experiments are of limited value. The normalized TKE is an order of magnitude greater compared to the experiments of Kitsikoudis et al. (2020). Within the results, solely trends can be seen. The cause of this high TKE is the threshold applied in combination with the quality of the data. As a result of a very low correlation and SNR on the transversal axis, a considerable amount of data points have been filtered out.

Reynolds Shear Stress Within the $-\overline{u\prime v\prime}$ plot in Figure 24, it is hard to distinguish exact patterns. Solely, the pattern $8D$ behind the downstream patch of the emergent patch has a clear pattern. The same pattern is present in the experiments of Kitsikoudis et al. (2020), where the staggered configuration with emergent patches was used. However, due to the limited amount of profiles confirming the same behaviour the conclusions should be considered of limited value.

Reynolds shear stress, $-\overline{u\prime w\prime}$, is shown behind the downstream submerged patch at $2D$ and $4D$. However, this shear of the vertical vortex is not present behind the upstream patch. This is remarkable, as a vertical vortex is also expected at the upstream submerged patch. Possibly, the steady wake region, and therefore the vertical vortex, would move closer to the patch due to the shortening of the steady wake region due to the jet flow. The influence of the downstream submerged patch on the upstream patch's steady wake is hard to confirm. The power spectral density analysis, in Figure 20, suggests that similar components within the flow influence the decay of turbulence, as the profiles are similar. However, in future research, confirmation of various analyses concluding the same behaviour would be desired.

Power Spectral Density Analysis To determine the behaviour of decay of turbulence a power spectral density analysis has been conducted for both emergent and submerged

configurations. This has been done behind both the upstream and downstream patches at the location of maximum transverse turbulence intensity. Determining the peak location in transverse turbulence intensity more accurately, using the recorded data itself instead of reference studies and data, would have given more confident results about the power of the Von Karman vortex streets behind the patches. Having high-quality data recordings would not only lead to more certain conclusions, but additionally, the peak within the spectral density analysis would have been more useful if less noise was present within the data.

Within the power spectral density analysis, the peaks are not present as in the studies of Liu et al. (2018) where of isolated patches have been studied. The authors' study shows how the peaks can show the vortex shedding behind the patches and the presence of a Von Karman vortex street. In Liu et al. (2018) study, a submerged patch had a less pronounced peak, indicating a less significant Von Karman vortex street. Differences in the current study could not be distinguished in the power spectral density analyses within the results.

These power spectral density analyses have each been done at the location with the peak transverse turbulence intensity. For emergent and submerged in the study of Liu et al. (2018) respectively, $1.1D$ and $2.4D$ behind the patch on the centerline. These distances of peak transverse turbulence intensity behind the patch are not close to the results of the acquired data of the NIOZ. When analyzing the difference between the spectral density analysis, with filter thresholds 15% correlation and 4 dB SNR, in an emergent and submerged configuration, differences are present within the profiles.

For the emergent configuration, the power spectral density analysis profiles are present in Figures 19. The upstream patch power spectral density analysis profile is of less power compared to the downstream patch power spectral density analysis profile, indicating disruption of the Von Karman vortex street. It needs to be noted that the location behind the upstream patch is determined using the results of Kitsikoudis et al. (2020) and Liu et al. (2018) so this claim is not certain. The disturbance of the Von Karman vortex street, of the upstream patch, is nevertheless consistent with the trends and patterns in the profiles of Figure 23. In Figure 23, the jet flow can be observed, which can shorten the steady wake region.

For the submerged configuration, it can be observed that the upstream and downstream Von Karman vortex streets are disturbed. This can be seen, as the profiles of the power spectral density analysis for the upstream and downstream patch have the same decay of turbulence, as seen in Figure 20. Therefore, it can that be both patches are influenced by the vortex of the flow over the top of the fully submerged patch and not the jet flow. When the jet flow influences the upstream patch's steady wake region the profiles would differ. Just like the shortening/disturbance of the patches, a steady wake region is consistent with the conclusions of Liu et al. (2018).

However, a significant difference in peaks cannot be observed in the peaks of the emergent and submerged configurations, in Figure 19 and 20, as seen in the research of Hu et al. (2018) and Liu et al. (2018). Indicating the difference in the shedding behaviour, by the significance of the peak, would be of value in determining the difference in emergent and submerged patches' shedding behaviour. As there is no peak observed, it cannot be seen if the patch has the same shedding frequency as a solid cylinder like in the research of Kitsikoudis et al. (2020) and Zong and Nepf (2012) showed.

Data Quality Having adequate data quality will help to interpret water flow behaviour more effortlessly compared to data which is greatly contaminated. The quality of the data collected was analyzed. The submerged configuration amount of data points remaining after applying the filter threshold and before despiking is much lower compared to the emergent data. For the transverse velocity, the number of data points valid for the emergent and fully submerged configurations, respectively, are 48.3% and 30.9%. Because of this, the emergent patch configuration has a higher degree of confidence in the chosen location of peak transverse turbulence intensity than the fully submerged configuration. This difference makes comparing the emergent and submerged configurations' data more challenging. The comparison will be more challenging because the amount if white noise will influence the power spectral density analysis.By carrying out additional research, the significance of the Von Karman vortex street can be determined with greater confidence.

Implications Results on Evolution Patches Deposition experiments have not been done within this research, however, this is of great interest for the evolution of patches and ecosystems (Sand-Jensen & Mebus, 1996). In the literature, research has been done on the deposition within steady wake regions of patches (Follett & Nepf, 2012; Liu et al., 2018; Meire et al., 2014). For emergent patches in a staggered configuration, it is known the upstream steady wake region is affected by the downstream patch (Kitsikoudis et al., 2020). Therefore, influencing the region with enhanced deposition, having lower TKE and reduced flow velocity (Liu et al., 2018).

The results show that recirculation is enhanced with submerged patches due to the vertical vortex. If deposition experiments are conducted in future research, it is likely that the upstream and downstream submerged patches, with $h/H = 0.5$, will have the same steady wake region length, as pointed out in the power spectral density analysis paragraph. Due to this vertical vortex evolution of patches will be more challenging compared to emergent patches.

6 Conclusion

Flow-vegetation feedback of submerged rigid vegetation in staggered configurations is an area of research which has not been explored yet in the literature to date. This knowledge gained can be applied in the exploration of the implementation of macrophytes to enhance the management and conservation of macrophytes.

In this study, data quality and filtering played an important role in the choices made. An understanding of the data collected at the NIOZ in Yerseke is crucial to being confident in the conclusions and recommendations made. Data filtering can have a significant result on the data and the patterns preserved. The most important axis in determining the start of a Von Karman vortex street, v axis, was of the lowest quality, with below 50% of the data points remaining after filtering with the used threshold. This threshold had turbulence dissipation closest to the -5/3 law. However, as a result of the limited amount valid of data points left, the average flow is the most reliable within the analyses done. Taking out valid data points results in less accuracy in determining fluctuations but the average flow velocity will remain within the data. The conclusions of the other flow characteristics analyzed, like TKE, should be considered of limited value.

The filter threshold applied before despiking, 15 correlation - 4 dB SNR, is an optimized fit for the cascade of turbulence on the transverse axis, u. However, it needs to be noted that the other axes have more data points above the filter threshold. As seen in the appendices, for most recordings with the applied filter threshold, over 80% of the data points are kept. Applying higher filter thresholds before despiking the data less valid data points will be kept. This will therefore influence the noise kept within the data. This noise can be seen in the power spectral density analysis where the high frequencies show a near horizontal line, especially the submerged configurations analysis, indicating noise. Greater amounts of noise will result in greater TKE. Therefore with very low filter thresholds solely the main patterns and trends can be taken into account within the results.

Within the results, jet flow is more dominant for the submerged configuration compared to the emergent staggered configuration. This is counterintuitive, as an emergent catch causes greater deflection of flow, as shown in the experiments of Liu et al. (2018). Like submerged isolated patches, vertical vortexes are present with the submerged configuration. The submerged configurations show greater turbulence average turbulence in all instances in the longitudinal profiles. This is not in line with the isolated submerged patch experiments of Liu et al. (2018) where emergent patches caused greater turbulence overall, except closer to the patch due to the larger steady wake region. The transversal profiles show greater recirculation of the submerged patch, due to the vertical vortex, this being in line with the findings on isolated patch experiments (Liu et al., 2018; Sadeque et al., 2008, 2009). Compared to the upstream patch, the downstream patch has greater turbulence. This is likely due to the mixing which already taken place upstream from the patch. Shortening of the upstream steady wake region makes it hard to distinguish between the emergent and submerged configurations due to the low quality of the data. The power spectral density analyses however suggest that the submerged patch's steady wake regions are both mostly influenced by the vertical vortex, as both upstream and downstream profiles show similar patterns. On the other hand, the emergent power spectral density analysis shows a profile with greater values in the downstream profile compared to the upstream profile. Therefore suggesting disturbance of the upstream steady wake region by the jet flow between the patches.

This study has given an exploration into staggered submerged rigid patch configurations. The evolution of patches due to the deposition of, for example, propagules will not benefit from the increased turbulence introduced by vertical vortexes into the flow. Compared to emergent staggered patch configurations, the steady wake region will shorten the submerged patch configuration. The findings underscore the importance of sufficient data quality to have greater results and more confidence in the conclusions drawn in this research. However, this research lays the foundation for further exploration of the complex interaction of flow-vegetation-sediment feedback.

In future research, it is important to have extensive knowledge of rigid submerged patches in staggered configuration before going towards flexible stemmed patches in staggered configuration. In the discussion, various possibilities have been suggested for future research. However, only one submerged h/H ratio has been considered in this research. It is important to know at which h/H ratio the vertical vortex is dominant for the length of the steady wake region in a staggered configuration. This distance is helpful in the development of ecosystems as grouped patches will need to form a synergy instead of behaving as isolated patches with the development.

References

Baattrup-Pedersen, A., & Riis, T. (1999). Macrophyte diversity and composition in relation to substratum characteristics in regulated and unregulated danish streams. *Freshwater Biology*, *42*(2), 375–385. https://doi.org/10.1046/j.1365-2427.1999.444487.x

Bornette, G., & Puijalon, S. (2011). Response of aquatic plants to abiotic factors: A review. *Aquatic sciences*, *73*, 1–14. https://doi.org/10.1007/s00027-010-0162-7

Bouma, T., De Vries, M., Low, E., Peralta, G., Tánczos, I. v., van de Koppel, J., & Herman, P. M. J. (2005). Trade-offs related to ecosystem engineering: A case study on stiffness of emerging macrophytes. *Ecology*, *86*(8), 2187–2199. https://doi.org/10.1890/04-1588

Bytyçi, P., Shala-Abazi, A., Zhushi-Etemi, F., Bonifazi, G., Hyseni-Spahiu, M., Fetoshi, O., Çadraku, H., Feka, F., & Millaku, F. (2022). The macrophyte indices for rivers to assess the ecological conditions in the klina river in the republic of kosovo. *Plants*, *11*(11), 1469. https://doi.org/10.3390/plants11111469

Chambers, P., Lacoul, P., Murphy, K., & Thomaz, S. (2008). Global diversity of aquatic macrophytes in freshwater. *Freshwater animal diversity assessment*, 9–26. https://doi.org/10.1007/978-1-4020-8259-7_2

Chen, L., Tu, J., & Yeoh, G. (2003). Numerical simulation of turbulent wake flows behind two side-by-side cylinders. *Journal of fluids and structures*, *18*(3-4), 387–403. https://doi.org/10.1016/j.jfluidstructs.2003.08.005

Chen, Z., Jiang, C., & Nepf, H. (2013). Flow adjustment at the leading edge of a submerged aquatic canopy. *Water Resources Research*, *49*(9), 5537–5551. https://doi.org/10.1002/wrcr.20403

Chen, Z., Ortiz, A. C., Zong, L., & Nepf, H. (2012). The wake structure behind a porous obstruction and its implications for deposition near a finite patch of emergent vegetation. *Water Resources Research*. https://doi.org/10.1029/2012WR012224

Christiansen, T., Azlak, M., Ivits-Wasser, E., et al. (2019). Floodplains: A natural system to preserve and restore. *EEA Report*, (24/2019).

Cornacchia, L., Folkard, A., Davies, G., Grabowski, R. C., van de Koppel, J., van der Wal, D., Wharton, G., Puijalon, S., & Bouma, T. J. (2019a). Plants face the flow in v formation: A study of plant patch alignment in streams. *Limnology and oceanography*, *64*(3), 1087–1102. https://doi.org/10.1002/lno.11099

Cornacchia, L., Licci, S., Nepf, H., Folkard, A., van der Wal, D., van de Koppel, J., Puijalon, S., & Bouma, T. J. (2019b). Turbulence-mediated facilitation of resource uptake in patchy stream macrophytes. *Limnology and Oceanography*, *64*(2), 714–727.

Danley, B., & Widmark, C. (2016). Evaluating conceptual definitions of ecosystem services and their implications. *Ecological Economics*, *126*, 132–138. https://doi.org/10.1016/j.ecolecon.2016.04.003

De Lima, P. H., Janzen, J. G., & Nepf, H. M. (2015). Flow patterns around two neighboring patches of emergent vegetation and possible implications for deposition and vegetation growth. *Environmental Fluid Mechanics*, *15*(4), 881–898. https://doi.org/10.1007/s10652-015-9395-2

European Commission. (2023). Water Framework Directive [Accessed on 7 June 2023].

Follett, E. M., & Nepf, H. M. (2012). Sediment patterns near a model patch of reedy emergent vegetation. *Geomorphology*, *179*, 141–151.

Forman, R. T. (1995). Some general principles of landscape and regional ecology. *Landscape ecology*, *10*, 133–142. https://doi.org/10.1007/BF00133027

Franca, M. J., & Brocchini, M. (2015). Turbulence in rivers. *Rivers–Physical, fluvial and environmental processes*, 51–78. https://doi.org/10.1007/978-3-319-17719-9_2

Goring, D. G., & Nikora, V. I. (2002). Despiking acoustic doppler velocimeter data. *Journal of hydraulic engineering*, *128*(1), 117–126. https://doi.org/10.1061/(ASCE)0733-9429(2002)128:1(117)

Grenier, E. (2004). Boundary layers. *Handbook of mathematical fluid dynamics*, *3*, 245–309.

Hu, Z., Lei, J., Liu, C., & Nepf, H. (2018). Wake structure and sediment deposition behind models of submerged vegetation with and without flexible leaves. *Advances in Water Resources*, *118*, 28–38. https://doi.org/10.1016/j.advwatres.2018.06.001

Jakubínskỳ, J., Prokopová, M., Raška, P., Salvati, L., Bezak, N., Cudlín, O., Cudlín, P., Purkyt, J., Vezza, P., Camporeale, C., et al. (2021). Managing floodplains using nature-based solutions to support multiple ecosystem functions and services. *Wiley Interdisciplinary Reviews: Water*, *8*(5), e1545. https://doi.org/10.1002/wat2.1545

Jesson, M. A., Bridgeman, J., & Sterling, M. (2015). Novel software developments for the automated post-processing of high volumes of velocity time-series. *Advances in Engineering Software*, *89*, 36–42. https://doi.org/10.1016/j.advengsoft.2015.06.007

Kitsikoudis, V., & Huthoff, F. (2022). River flow processes: Lecture notes.

Kitsikoudis, V., Kirca, V. O., Yagci, O., & Celik, M. F. (2017). Clear-water scour and flow field alteration around an inclined pile. *Coastal Engineering*, *129*, 59–73. https://doi.org/10.1016/j.coastaleng.2017.09.001

Kitsikoudis, V., Yagci, O., & Kirca, V. O. (2020). Experimental analysis of flow and turbulence in the wake of neighboring emergent vegetation patches with different densities. *Environmental fluid mechanics*, *20*(6), 1417–1439. https://doi.org/10.1007/s10652-020-09746-6

Kitsikoudis, V., Yagci, O., Kirca, V. O., & Kellecioglu, D. (2016). Experimental investigation of channel flow through idealized isolated tree-like vegetation. *Environmental Fluid Mechanics*, *16*, 1283–1308. https://doi.org/10.1007/s10652-016-9487-7

Kolmogorov, A. N. (1941a). Dissipation of energy in the locally isotropic turbulence. *Dokl. Akad. Nauk. SSSR*, *32*, 19–21. https://doi.org/10.1098/rspa.1991.0076

Kolmogorov, A. N. (1941b). The local structure of turbulence in incompressible viscous fluid for very large reynolds. *Numbers. In Dokl. Akad. Nauk SSSR*, *30*, 301. https://doi.org/10.1098/rspa.1991.0075

Kuhar, U., Germ, M., Gaberščik, A., & Urbanič, G. (2011). Development of a river macrophyte index (rmi) for assessing river ecological status. *Limnologica*, *41*(3), 235–243. https://doi.org/10.1016/j.limno.2010.11.001

Kuo, H.-H. (2018). *White noise distribution theory*. CRC press. https://doi.org/10.1201/9780203733813

Lee, S., & Harsha, P. (1970). Use of turbulent kinetic energy in free mixing studies. *AIAA journal*, *8*(6), 1026–1032. https://doi.org/10.2514/3.5826

Liu, C., Hu, Z., Lei, J., & Nepf, H. (2018). Vortex structure and sediment deposition in the wake behind a finite patch of model submerged vegetation. *Journal of Hydraulic Engineering*, *144*(2), 04017065. https://doi.org/10.1061/(ASCE)HY.1943-7900.0001408

Madsen, J. D., Chambers, P. A., James, W. F., Koch, E. W., & Westlake, D. F. (2001). The interaction between water movement, sediment dynamics and submersed macrophytes. *Hydrobiologia*. https://doi.org/10.1023/a:1017520800568

Meire, D., Kondziolka, J. M., & Nepf, H. (2014). Interaction between neighboring vegetation patches: Impact on flow and deposition. *Water Resources Research*. https://doi.org/10.1002/2013wr015070

Micheli, E., & Kirchner, J. (2002). Effects of wet meadow riparian vegetation on streambank erosion. 2. measurements of vegetated bank strength and consequences for failure mechanics. *Earth surface processes and landforms: the journal of the British Geomorphological Research Group*, *27*(7), 687–697. https://doi.org/10.1002/esp.340

Milliman, J. D., & Syvitski, J. P. (1992). Geomorphic/tectonic control of sediment discharge to the ocean: The importance of small mountainous rivers. *The journal of Geology*, *100*(5), 525–544. https://doi.org/10.1086/629606

Müller, P. (2006). *The equations of oceanic motions*. Cambridge University Press. https://doi.org/10.5670/oceanog.2007.73

Nepf, H. M. (2012). Flow and transport in regions with aquatic vegetation. *Annual review of fluid mechanics*, *44*, 123–142. https://doi.org/10.1146/annurev-fluid-120710-101048

Nortek Group. (2021). *What are weak spots and how can I avoid them?*

Nortek Group. (2022). Comprehensive Manual for Velocimeters.

Nortek Group. (n.d.). Vectrino User Manual.

Ortiz, A. C., Ashton, A. D., & Nepf, H. (2013). Mean and turbulent velocity fields near rigid and flexible plants and the implications for deposition. *Journal of Geophysical Research*. https://doi.org/10.1002/2013jf002858

Richardson, L. F. (1920). The supply of energy from and to atmospheric eddies. *Proceedings of the Royal Society of London. Series A, Containing Papers of a Mathematical and Physical Character*, *97*(686), 354–373. https://doi.org/10.1098/rspa.1920.0039

Sadeque, M., Rajaratnam, N., & Loewen, M. (2008). Flow around cylinders in open channels. *Journal of engineering mechanics*, *134*(1), 60–71. https://doi.org/10.1061/(ASCE)0733-9399(2008)134:1(60)

Sadeque, M., Rajaratnam, N., & Loewen, M. (2009). Effects of bed roughness on flow around bed-mounted cylinders in open channels. *Journal of Engineering Mechanics*, *135*(2), 100–110. https://doi.org/10.1061/(ASCE)0733-9399(2009)135:2(100)

Sand-Jensen, K., Andersen, K., & Andersen, T. (1999). Dynamic properties of recruitment, expansion and mortality of macrophyte patches in streams. *International review of hydrobiology*, *84*(5), 497–508. https://doi.org/10.1002/iroh.199900044

Sand-Jensen, K., & Mebus, J. R. (1996). Fine-scale patterns of water velocity within macrophyte patches in streams. *Oikos*, 169–180. https://doi.org/10.2307/3545759

Scheffer, M., Carpenter, S., Foley, J. A., Folke, C., & Walker, B. (2001). Catastrophic shifts in ecosystems. *Nature*, *413*(6856), 591–596.

Schoelynck, J., Creëlle, S., Buis, K., De Mulder, T., Emsens, W.-J., Hein, T., Meire, D., Meire, P., Okruszko, T., Preiner, S., et al. (2018). What is a macrophyte patch? patch identification in aquatic ecosystems and guidelines for consistent delineation. *Ecohydrology & Hydrobiology*, *18*(1), 1–9. https://doi.org/10.1016/j.ecohyd.2017.10.005

Shalaby, H. H. (2007). On the potential of large eddy simulation to simulate cyclone separators.

Smits, A. J. (2000). Lectures in fluid mechanics: Viscous flows and turbulence. *Department of Mechanical Engineering Princeton University*.

Sumner, D. (2010). Two circular cylinders in cross-flow: A review. *Journal of fluids and structures*, *26*(6), 849–899. https://doi.org/10.1016/j.jfluidstructs.2010.07.001

Takemura, T., Takemura, T., & Tanaka, N. (2007). Flow structures and drag characteristics of a colony-type emergent roughness model mounted on a flat plate in uniform flow. *Fluid Dynamics Research*. https://doi.org/10.1016/j.fluiddyn.2007.06.001

Thomaz, S. M., & Cunha, E. R. (2010). The role of macrophytes in habitat structuring in aquatic ecosystems: Methods of measurement, causes and consequences on animal assemblages' composition and biodiversity. *Acta Limnologica Brasiliensia*. https://doi.org/10.4322/actalb.02202011

Vandenbruwaene, W., Temmerman, S., Bouma, T., Klaassen, P., De Vries, M., Callaghan, D., Van Steeg, P., Dekker, F., Van Duren, L., Martini, E., et al. (2011). Flow interaction with dynamic vegetation patches: Implications for biogeomorphic evolution of a tidal landscape. *Journal of Geophysical Research: Earth Surface*, *116*(F1). https://doi.org/10.1002/lno.11070

van Vliet, M. T., Franssen, W. H., Yearsley, J. R., Ludwig, F., Haddeland, I., Lettenmaier, D. P., & Kabat, P. (2013). Global river discharge and water temperature under climate change. *Global Environmental Change*, *23*(2), 450–464. https://doi.org/10.1016/j.gloenvcha.2012.11.002

Wang, J., He, G., Dey, S., & Fang, H. (2022). Influence of submerged flexible vegetation on turbulence in an open-channel flow. *Journal of Fluid Mechanics*, *947*, A31. https://doi.org/10.1017/jfm.2022.598

Yagci, O., Celik, M. F., Kitsikoudis, V., Kirca, V. O., Hodoglu, C., Valyrakis, M., Duran, Z., & Kaya, S. (2016). Scour patterns around isolated vegetation elements. *Advances in Water Resources*, *97*, 251–265. https://doi.org/10.1016/j.advwatres.2016.10.002

Yagci, O., Özgur Kirca, V., Kitsikoudis, V., Wilson, C. A., Celik, M. F., & Sertkan, C. (2024). Experimental study on influence of different patterns of an emergent vegetation patch on the flow field and scour/deposition processes in the wake region. *Water Resources Research*, *60*(1). https://doi.org/10.1029/2023WR034978

Yamasaki, T. N., Jiang, B., Janzen, J. G., & Nepf, H. M. (2021). Feedback between vegetation, flow, and deposition: A study of artificial vegetation patch development. *Journal of Hydrology*, *598*, 126232. https://doi.org/10.1016/j.jhydrol.2021.126232

Zakharov, V. E., L'vov, V. S., & Falkovich, G. (2012). *Kolmogorov spectra of turbulence i: Wave turbulence*. Springer Science & Business Media.

Zong, L., & Nepf, H. (2012). Vortex development behind a finite porous obstruction in a channel. *Journal of Fluid Mechanics*. https://doi.org/10.1017/jfm.2011.479

A Filter Threshold Tables

Table 5: Data sets against filter thresholds correlation-SNR combinations percentage good u axis.

Label	**T/TestNumber**	**10-3**	**15-4**	**20-5**	**30-7**	**40-10**
E1	'00029'	98.22	95.62	87.93	64.72	35.89
E2	'00032'	96.84	93.33	84.81	63.98	34.69
E3	'00034'	98.73	96.78	91.18	76.30	54.28
S1	'00036'	80.16	69.09	52.93	27.02	11.63
S2	'00037'	93.33	88.17	75.25	49.16	23.84
S3	'00038'	97.46	93.84	84.12	64.95	29.53
S1	'00039'	71.16	58.35	40.72	19.11	7.59

Table 6: Data sets against filter thresholds correlation-SNR combinations percentage good v axis.

Label	**T/TestNumber**	**10-3**	**15-4**	**20-5**	**30-7**	**40-10**
E1	'00029'	73.37	52.91	34.52	16.34	4.86
E2	'00032'	66.62	46.25	31.36	16.14	5.92
E3	'00034'	66.16	45.73	31.69	17.91	9.10
S1	'00036'	51.96	26.89	12.79	4.52	1.32
S2	'00037'	58.60	33.51	17.32	5.83	1.99
S3	'00038'	56.97	32.22	16.61	5.90	2.48
S1	'00039'	46.90	22.29	9.41	2.95	0.75

Table 7: Data sets against filter thresholds correlation-SNR combinations percentage good w axis.

Label	**T/TestNumber**	**10-3**	**15-4**	**20-5**	**30-7**	**40-10**
E1	'00029'	90.37	81.03	63.27	34.25	15.37
E2	'00032'	92.12	86.21	76.19	50.17	27.82
E3	'00034'	95.39	90.51	79.97	56.22	34.85
S1	'00036'	65.16	50.54	33.46	14.20	5.03
S2	'00037'	87.32	79.06	65.95	38.93	17.67
S3	'00038'	88.46	78.45	64.03	34.73	16.30
S1	'00039'	58.64	43.48	26.67	9.44	3.65